Optical Limiting via Plasmonic Parametric Absorbers

Eric Schweisberger

B.S. Electrical Engineering, University of Kansas, 2018

Submitted to the graduate degree program in Department of Electrical Engineering and Computer Science and the Graduate Faculty of the University of Kansas in partial fulfillment of the requirements for the degree of Master of Science.

Alessandro Salandrino, Chair

Committee members

Kenneth Demarest, Committee Member

Rongqing Hui, Committee Member

Date defended: January 30th, 2020

The Thesis Committee for Eric Schweisberger certifies
that this is the approved version of the following thesis :

Optical Limiting via Plasmonic Parametric Absorbers

Alessandro Salandrino, Chair

Date approved: January 30th, 2020

Abstract

Optical sensors are increasingly prevalent devices whose costs tend to increase with their sensitivity. A hike in sensitivity is typically associated with fragility, rendering expensive devices vulnerable to threats of high intensity illumination. These potential costs and even security risks have generated interest in devices that maintain linear transparency under tolerable levels of illumination, but can quickly convert to opaque when a threshold is exceeded. Such a device is deemed an optical limiter. Copious amounts of research have been performed over the last few decades on optical nonlinearities and their efficacy in limiting. This work provides an overview of the existing literature and evaluates the applicability of known limiting materials to threats that vary in both temporal and spectral width. Additionally, we introduce the concept of plasmonic parametric resonance (PPR) and its potential for devising a new limiting material, the plasmonic parametric absorber (PPA). We show that this novel material exhibits a reverse saturable absorption behavior and promises to be an effective tool in the kit of optical limiter design.

Acknowledgements

First and foremost, I would like to extend my most sincere gratitude toward the educators who have inspired and motivated me in the never-ending pursuit of knowledge: my graduate advisor and committee chair, Dr. Alessandro Salandrino, for continuous inspiration, for his phenomenal ability to make even the most perplexing of topics approachable by those of us less worthy, and, of course, for his time; my undergraduate advisor and career mentor, Dr. Shannon Blunt, for encouraging me to pursue a graduate degree and facilitating relationships with those who would become my eventual employers; Dr. Kenneth Demarest, the man who keeps the sense of rigor alive within the undergraduate curriculum, for teaching me the importance of being able to tell the whole story; Dr. Victor Frost for keeping the sense of awe alive in the devices that we take for granted every day; Prof. Daniel Martinez for his unapologetic sarcasm, his relentless energy in the classroom, and his ability to convey the most abstract of topics as mundane; and Prof. Brenda Edmonds for showing me the beauty in mathematics and, most importantly, that I am capable.

I would also like to thank my close friends, Nicci Bowman and Brian Terry, for their level-headed guidance and for holding me accountable throughout all of these years, my parents for the support that they have provided when I needed it the most, and all of those who have acted as mentors toward me while I have been on this journey. Finally, I acknowledge the National Science Foundation and the Scholarship for Service program that has provided me the opportunity to continue working toward a Masters of Science and set me on the trajectory of public service in the national interest.

Contents

List of Figures

Chapter 1

Introduction

The term optical limiting describes the action of manipulating light incident on a sensor so as to protect the sensor from permanent damage. This phenomenon is of increasing importance in the current technological era where optical sensors grow evermore prevalent. The heightened sensitivities of new sensor technologies paired with shrinking laser pulse timescales and increasing fluences brings further urgency to the field. Even photonic sensors that do not progress, such as the human eye, remain vulnerable to the weakest threats when systems of optical gain are placed in front of them for amplified viewing. Therefore, it is prudent to explore the realm of possibilities in which materials and devices can be recruited or engineered for optical limiting purposes. The first class of devices that comes to mind is the active limiter. These devices exhibit dynamic control of their limiting properties through some form of feedback. Unfortunately, by the very nature of their serial construction, dynamic devices are both complex and slow to respond to an incoming threat. They typically require communication between a sensor, a control module, and an actuator. This communication link inherently imposes delay between the arrival of the threat and the action of limiting, during which the incident energy may have already caused irreversible damage. Therefore, we look beyond active limiters to a group of passive devices. Such devices rely on nonlinear material properties to interact with the incident threat by absorbing, scattering, or dispersing the incoming field before it reaches the sensor. The only sense of delay in passive devices is the ability of the material to respond to the incident field. This response time is orders of magnitude smaller than that of an active system, resulting in fast optical limiters of simplistic design.

An effective optical limiter exhibits a threshold at which it constrains the incoming beam,

allowing only a fixed or very slowly increasing amount of energy to reach the sensor. When the incident fluence is below the limiting threshold, the material should appear transparent or transmit linearly so as not to interfere with the integrity of the desired signal. How the device responds once the threshold is reached depends on the nonlinear mechanism excited within.

Many material responses experience some time dependence and can therefore be used to manipulate incoming pulses within the time domain. These pulse shaping applications vary from low-pass filtering and pulse compression to background noise reduction in pulsed spectroscopy. In addition to protecting sensors from damage or destruction, optical limiters may also be used to expand a sensor's dynamic range through fluence dependent attenuation of the incoming field. Incident fields with large fluences are strongly attenuated while weak fields experience little attenuation, rendering a broader range of incident energies to be detectable.

Chapter 2

Optical Limiting Mechanisms: An Overview

Abstract

This chapter contains an overview of nonlinear mechanisms commonly employed within optical limiting materials. These mechanisms can be separated into four groups: nonlinear absorption, nonlinear refraction, induced scattering, and optically induced phase transitions. Nonlinear absorption phenomena include two-photon absorption, excited-state absorption, and free-carrier absorption. Nonlinear refraction occurs through molecular reorientation, the electronic Kerr effect, excitation of free carriers, photorefraction, and optically induced thermal heating. Induced scattering can be a consequence of optically induced heating or plasma generation and induced phase transitions are typically a consequence of thermal effects as well. The phenomenology of these material responses and their applications to passive optical limiting devices are explained within.

2.1 Instantaneous vs Accumulative Nonlinearities

The nonlinear mechanisms that generate limiting behavior in passive devices can be broadly associated with one of two groups: instantaneous nonlinearities or accumulative nonlinearities. Instantaneous nonlinearities are those in which the polarization density responds immediately to an applied electric field. These can be described by expanding the polarization density amplitude, P, as a Taylor's series about the electric field amplitude, E.

$$P = \varepsilon_0\left(\chi^{(1)}E + \chi^{(2)}EE + \chi^{(3)}EEE\right) \tag{2.1}$$

The first term, $\chi^{(1)}$, describes linear absorption and refraction. The higher order terms are associated with the weak nonlinear interactions and require strong incident electric fields if their effects are to be observed. The $\chi^{(2)}$ term exists only in noncentrosymmetric materials and is responsible for sum and difference frequency mixing, the Pockels electro-optic effect, and optical rectification. The $\chi^{(3)}$ term is associated with two-photon absorption and the electronic Kerr effect, both of which are common within limiting materials; the Kerr effect is associated with its real component and two-photon absorption is associated with its imaginary component. These instantaneous nonlinearities are non-resonant features and therefore respond to a large bandwidth of electric field. However, they require very high intensities and are typically only effective for very short pulses.

Accumulative nonlinearities exhibit polarization densities that are dependent on the previous state. These polarization densities are generated by an applied electric field but they grow and decay slowly, on the timescale of the excitation or longer. They depend on the cumulative amount of energy deposited into the medium over time rather than the intensity at a given instant. Since these effects are fluence dependent, they can be used to construct limiting materials with responses that are independent of pulse duration. Examples of accumulative nonlinearities include excited-state and free-carrier absorption as well as nonlinear refractive processes. The effects may even be non-local such as in the photorefractive effect. One caveat to these nonlinearities is that they are often highly resonant features and therefore only operate within a narrow bandwidth. Thus, the primary tradeoffs between instantaneous and accumulative nonlinearities are those of bandwidth and dependence on pulse duration.

2.2 Nonlinear Absorption

2.2.1 Reverse Saturable Absorption

The first mechanism that we investigate is a form of excited-state absorption known as reverse saturable absorption (RSA). Prior to the discovery of RSA, interest was generated around the opposite effect, saturable absorption. A saturable absorber is a material that transitions from linearly

absorbing to transparent when exposed to intense illumination. The underlying cause of this phenomenon is understood by considering a system model of two discrete energy levels. The ground state is substantially populated while the excited state is sparsely populated. When the material is illuminated, the ground state electrons are excited to the higher energy state. Under illumination of sufficient intensity, the majority of the ground state electrons are excited such that they occupy the available higher energy states, thus depleting the ground state and reducing the probability of absorption. It is under this high-intensity illumination that the material loses the capacity to absorb additional photons and instead becomes transparent to the optical energy exceeding the threshold.

Having the opposite reaction, reverse saturable absorbers exhibit linear transmission at low intensities but become opaque under intense illumination. While these materials cannot be realized by a simple two-state system, the mechanism employed is similar in a system of three discrete energy levels. The defining characteristic that determines whether the three-level material behaves as a saturable absorber or a reverse saturable absorber is the ratio of the absorption cross-sections, σ_2/σ_1 [44]. The absorption cross-section between the ground state and the first excited state is σ_1 and the cross-section between the first and second excited states is σ_2. Under low intensity illumination, the ground state electrons are promoted to the first excited state. These excited states quickly decay back to the ground state before the band of the first excited states becomes full. Thus, a sufficient number of available excited states remains so that the material exhibits a linearly absorbing behavior according to the Beer-Lambert law. The population at the first band of excited states becomes of concern when illumination intensity is sufficiently high. If the first excited band becomes full and $\sigma_1 > \sigma_2$, then the material loses the ability to absorb additional photons, bleaching to transparency just like the two-level saturable absorber. However, if $\sigma_2 > \sigma_1$, then the probability of electrons in the first excited state being promoted to the second excited state exceeds the probability of ground state to excited state absorption. The result is a substantial number of available states in the first excited band and an increase in absorption to the second excited band once the first begins to populate. Analysis of the relevant rate equations reveals that if the ratio σ_2/σ_1 is large, then the transmission of this material will become relatively constant

under sufficient illumination [44].

Though simple to analyze, the three-level system has its shortcomings. Most three-level materials consist of singlet states where all energy transitions are allowed. This results in large absorption cross-sections but small lifetimes. The rapid excited-state decay suggests that incident pulses on longer timescales require a persistently high intensity in order to maintain activation of the nonlinearity through population of the excited state. A solution to this lies in materials that allow intersystem crossing from the first excited state. An example is the five-level diagram in Figure 2.1 where the fourth level is reached by intersystem crossing from the first excited state (denoted 2). This energy level is typically a triplet or other long-lived state that accumulates population over a greater timescale. If the rate of transition to the fourth level is sufficiently high, and the absorption cross-section from the fourth to the fifth state is also large, then the RSA will effectively suppress pulses on the timescale of the fourth state's lifetime τ_4.

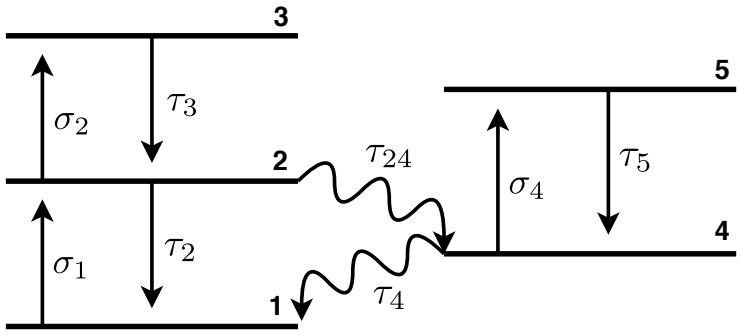

Figure 2.1: Five-level Energy Diagram with Intersystem Crossing

2.2.2 Two-Photon Absorption

Two-photon absorption (TPA) is an instantaneous nonlinearity in which two photons are absorbed simultaneously. The first promotes an electron to an intermediate energy level. This can be thought of as the first excited state of the three-level RSA model with a lifetime approaching zero. The second photon promotes the electron from the intermediate energy level to the final excited state at the sum of the energies of the two photons. This is a fast-acting phenomenon, on the order of an

optical cycle, and is independent of pulse length provided a fixed intensity of sufficient magnitude. The intensity as the beam travels through a material can be described by (2.2) where α is the linear absorption coefficient. The TPA coefficient, β, is described by (2.3) [44] where c is the speed of light in vacuum, n_0 is the linear index of refraction, and ω is the angular frequency of the incident field.

$$\frac{\partial I}{\partial z} = -(\alpha + \beta I)I \tag{2.2}$$

$$\beta = \frac{3\omega}{2\varepsilon_0 c^2 n_0^2} \operatorname{Im}\left[\chi^{(3)}\right] \tag{2.3}$$

For a transparent material (i.e. at low intensities), the linear absorption is small. If we solve Eq. 1 for $\alpha = 0$ then we arrive at the solution in (2.4).

$$\frac{I_0}{1 + I_0 \beta L} \tag{2.4}$$

It is from this equation that we derive the notion of limiting behavior. As the input intensity I_0 grows for a given material length L, the relative output intensity I grows more slowly and asymptotically approaches $\frac{1}{\beta L}$. The response clearly depends on the TPA coefficient β which is shown in (2.3) to be proportional to the imaginary component of the third-order susceptibility term $\chi^{(3)}$. As was previously discussed, the magnitude of the high order susceptibility coefficients is vanishingly small for increasing order. Thus, the magnitude of β is limited in existing materials and the resulting output intensity may be large for a limiting application. Since intensity is energy density divided by pulse duration, we can deduce that limiting with TPA alone is likely to be effective only for short pulses. This can be further illustrated by considering the output fluence when the input intensity I_0 is large ($I_0 \gg \beta L$) as in (2.5) where τ is the pulse duration. Here, we see that the transmitted energy is pulse duration dependent but independent of input intensity. This is an important consideration for limiting in applications such human eye protection where the threshold for damage is one of energy density.

$$F = \frac{\tau}{\beta L} \tag{2.5}$$

Also prudent for consideration are the effects of a nonuniform spatial beam profile. The previous analysis is performed by assuming a rectangular pulse in time and a cylindrically uniform spatial profile. If we consider the more realistic Gaussian spatial profile then the transmission of the sample can be shown to be [44]:

$$T = \frac{1}{\beta I_0 L} \ln\left[1 + \beta I_0 L\right] \tag{2.6}$$

where T is the transmission coefficient, relating output fluence to input fluence as dependent on the incident intensity. The decreasing energy density in the tails of the Gaussian beam profile results in areas of the TPA medium where TPA action does not occur. These rings of low intensity allow the incident intensity to pass through in a linear fashion, thus allowing the continued rise in output fluence with increasing input. It is this nature of the nonuniform beam profile that prevents a TPA material from truly clamping the output at a constant intensity – a necessary feature for an application such as eye protection.

2.2.3 Free-Carrier Absorption

Free-carrier absorption involves the absorption of incoming photons by free carriers in the absorbing material. For example, when single or two-photon absorption promotes an electron to the conduction band, this electron may be promoted again to a higher state by absorption of another photon. This process can occur through direct energy transfer or indirectly with assistance from phonons within the material. The phonon-assisted process is known as free-carrier absorption. This is clearly an accumulative nonlinearity as it depends on the prior generation of free carrier populations within the conduction bands via absorption. If we assume only linear and free-carrier absorption, the function of intensity as it varies through the nonlinear medium can be described as:

$$\frac{\partial I}{\partial z} = -(\alpha + \sigma N) I \tag{2.7}$$

where α is the linear absorption coefficient, N is the number density of electron-hole pairs, and σ is the total (sum of electrons and holes) free-carrier absorption cross section. The free-carrier absorption cross section for each carrier type is described by [47]:

$$\sigma = \frac{e^2}{n_0 c \varepsilon_0 m^* \omega^2} \left\langle \frac{1}{\tau_m} \right\rangle \tag{2.8}$$

where e is the fundamental electric charge, m^* is the carrier's effective mass, and τ_m is the carrier's relaxation time. Ignoring processes of recombination and diffusion, the electron-hole density can be determined by the following:

$$\frac{\partial N}{\partial t} = \frac{\alpha I}{\hbar \omega} \tag{2.9}$$

It is through (2.9) that we see dependence of the electron-hole density on the incident intensity. This is the basis for the nonlinear effect: the free-carrier absorption mechanism relies on the carrier population whose time derivative is proportional to the intensity of the illumination. An analytical approximation to the transmission of the medium can be derived through the solution of (2.7) and (2.9) under the assumptions of weak nonlinear absorption and of spatially and temporally Gaussian pulses. The result, also neglecting surface reflections, is [8]:

$$T = \frac{T_0}{1 + (1 - T_0)\left[\frac{F_0 \sigma}{4h\nu}\right]} \tag{2.10}$$

where $T_0 = \exp(-\alpha L)$ is the linear absorption, F_0 is the incident fluence, and ν is the temporal frequency of the optical excitation. The presence of fluence in the denominator of (2.10) reveals the dependence on incident fluence rather than intensity. This produces a pulse duration independent transmission function under the aforementioned assumptions. In reality, diffusion and recombination processes occur and, given a long enough timescale, alter the availability of free-carrier populations. Therefore, the free-carrier absorption nonlinearity does not produce a device response that is truly independent of pulse width. Equation (2.10) was also derived under the small-signal limit in which the nonlinear absorption can be ignored. This is not a practical assumption in

optical limiting assumptions due to the strong electric fields involved. Rather, (2.7) and (2.9) can be solved under the strong-signal limit to obtain [8]:

$$T = T_0 \left(\frac{F_c}{F_0} \right) \ln \left(1 + \frac{F_0}{F_c} \right) \tag{2.11}$$

$$F_c = \frac{2\hbar\omega}{\sigma(1 - T_0)} \tag{2.12}$$

where F_c is known as the critical fluence. Equations (2.11) and (2.12) further reveal the complexity of modeling transmission under free-carrier absorption. This effect alone is not significant enough to be the primary mechanism of nonlinear absorption in an optical limiting device. Nonetheless, it is present in semiconductor materials often used for optical limiting and its inclusion is necessary for precise modeling of these devices.

2.3 Nonlinear Refraction

Quite separate from absorptive limiting techniques, nonlinear refraction in a material poses the opportunity to change the spatial profile of an incoming threat. The nonuniform spatial profile of an incoming beam interacts with the material and causes a change in refractive index that is distributed proportionally to the spatial profile of the beam's intensity. Typically, the profile is of greatest intensity at the center and weakens radially. This results is a lensing effect that causes the transmitted beam to focus or defocus depending on the sign of the refractive index change. An aperture is placed on the transmission side of the nonlinear material and sized appropriately so as to create little loss when the index of the material is constant. When a beam of sufficient intensity interacts with the material, the lensing effect changes the waist location of the beam and causes the diverging spatial profile to spread over the blocking aperture. The intensity or fluence transmitted through the aperture is therefore reduced, protecting a sensor located on the opposite side. The diagram in Fig. 2.2 illustrates a simple device design where the incoming beam is focused on the nonlinear medium through a converging lens. The optical gain of the lens enables tuning

for the intensity threshold at which the device is activated. Under sub-threshold illumination, the refracting medium behaves linearly and is effectively transparent. When the incoming beam surpasses the threshold, the medium either defocuses directly on to the aperture as shown in Figure 2.2a or focuses to a nearer waist location before diverging onto the aperture as in Figure 2.2b. The choice of configuration is dependent on the sign of the refractive index change in the nonlinear medium.

The change in index profile can be represented analytically under a few simplifying assumptions. If the spatial profile of the beam is Gaussian and the change in index is linearly proportional to the intensity or fluence of the excitation, then the index change is:

$$\Delta n = \frac{\Delta n_0 e^{-2r^2}}{\omega_0^2} \cong \Delta n_0 \left(1 - \frac{2r^2}{a\omega_0^2}\right) \tag{2.13}$$

where Δn_0 is the change in on-axis index, r is the radial distance from the axis, ω_0 is the waist of the beam's E-field, and a is a correction term for the higher order terms of the Taylor series. A thin material of thickness L with this profile under the paraxial wave approximation yields a thin lens with focal length f [44]:

$$f = \frac{a\omega_0^2}{4(\Delta n)L} \tag{2.14}$$

Equation (2.14) reveals the inverse relationship between focal length and the nonlinearity. As the index change Δn increases in magnitude, the focal length is reduced. Since the change in index is assumed proportional to the illuminating intensity, an increase in incident fluence reduces the focal length, thereby decreasing the intensity incident upon the aperture. The sign of the index change determines whether the focal point is negative, located between the lens and the nonlinear medium, or positive and located between the medium and the aperture. A negative focal length produces a self-defocusing device (Fig. 2.2a) while a positive index change results in self-focusing (Fig. 2.2b). The choice of focusing versus defocusing media is dependent upon device performance requirements. The tendency of a focusing medium to further spatially confine the beam results in greater local intensities inside of the medium. While this increases the sensitivity of the nonlin-

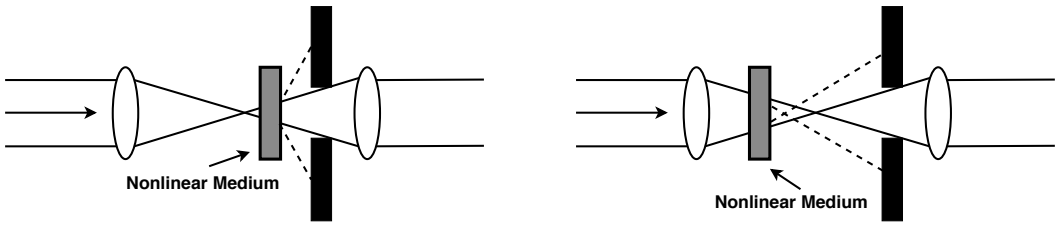

(a) Defocusing (b) Focusing

Figure 2.2: Nonlinear Refraction – Limiting Device Configurations

earity to low intensity illumination, this may also lead to irreversible damage to the medium when incident fluence is high. Defocusing media reduce local intensities inside the nonlinear medium and are generally safer as they may provide a self-protection mechanism for the limiter [23].

This discussion and supporting equations (2.13) and (2.14) are an oversimplification for the sake of illustration. In reality, multiple mechanisms within a material contribute to nonlinear refraction. In addition to the instantaneous $\chi^{(3)}$ response, local generation of free-carriers may contribute to the change in index and further complication lies in the potential for significant nonlinear absorption. The dependency on an accumulative nonlinearity reveals that the index change cannot be a simple linear function of the incident intensity. Furthermore, the determination of focal length under the paraxial approximation neglects the Gaussian nature of the induced lens. A more realistic scenario is considered where both instantaneous and accumulative responses contribute to nonlinear refraction within a material that exhibits TPA. The optical limiting action is therefore the sum of nonlinear absorption (TPA) effects and nonlinear refraction due to both the Kerr nonlinearity and carrier generation by TPA. According to Tutt & Boggess [44], the strength of the Kerr response can be characterized by the constant γ, described within an isotropic medium as:

$$\gamma = \frac{3}{4}\left(\frac{\mu_0}{\varepsilon_0}\right)^{1/2} \frac{\mathrm{Re}\left[\chi^{(3)}\right]}{n_0^2} \tag{2.15}$$

The resulting change in index is determined at the point of peak intensity I_0 as:

$$\Delta n_{Kerr} = \gamma I_0 \tag{2.16}$$

It has been shown by Sheik-Bahae et al. [41] that γ can be reliably predicted for photon energies below $\sim 0.8E_g$ where E_g is the bandgap energy. These results paired with the characterization of TPA dispersion [43] provide the following insight into the behavior of (2.16): γ has a magnitude dependence of E_g^{-4}, changes sign from positive to negative as the photon energy surpasses $0.7E_g$, and peaks near the TPA absorption edge. The assembly of this information provides a more accurate model of the Kerr nonlinearity and resulting index change.

Unlike the instantaneous index change in (2.16), nonlinear refraction due to carrier generation is not intensity dependent. Instead, this accumulative nonlinearity is a function of carrier density. The simplest model relates the accumulative index change as directly proportional to the carrier density N:

$$\Delta n_{FC} = n_{eh} N \tag{2.17}$$

where n_{eh} is the index change per photogenerated carrier pair. In a model that assumes two parabolic bands within a direct bandgap semiconductor, this is [5]:

$$n_{eh} = -\frac{e^2}{2n_0\varepsilon_0 m_{eh}}\left(\frac{1}{\omega^2} - \frac{1}{\omega^2 - \omega_g^2}\right) \tag{2.18}$$

where m_{eh} is the effective mass of the electron-hole pair and ω_g is the bandgap frequency. The TPA generated carrier density can be derived from (2.2) when $\alpha = 0$ as [44]:

$$\frac{\partial N}{\partial t} = \frac{\beta I^2}{2\hbar\omega} \tag{2.19}$$

which, for a rectangular pulse of intensity I_0 and duration τ, yields:

$$N = \frac{\tau\beta I_0^2}{2\hbar\omega} \tag{2.20}$$

Equation (2.20) shows that the carrier density is directly proportional to the duration of the excitation. This confirms the accumulative and duration-dependent nature of the variation in refractive index when inserted into (2.17). The competition between the two terms in (2.18) respectively represents intraband and interband (at ω_g) contributions. When the frequency of the excitation is below the bandgap frequency, the latter term is negative and contributes a net gain to the change in index. This term grows in magnitude as it approaches ω_g, reaching a maximum just below the bandgap energy. For optical frequencies just beyond the bandgap, this term is maximally positive and negates the intraband contribution, driving the sum toward zero as ω continues increasing. This model provides clear insight to the resonant nature of the change in index as the optical excitation frequency approaches the bandgap energy from below. The enhancement of this accumulative nonlinearity must be taken into consideration when evaluating the dominant effect in a limiting application.

Comparison of the instantaneous and accumulative nonlinearities reveals that the contributions by carrier generation are effectively fifth order [44] while the Kerr nonlinearity is a third order response. This implies that the accumulative nonlinearity will dominate beyond some critical level of excitation. Equating (2.16) and (2.17) allows for an estimation of this critical excitation level in terms of fluence, F_c':

$$F_c' = \frac{\gamma}{n_{eh}} \frac{2\hbar\omega}{\beta} \tag{2.21}$$

When the incident excitation exceeds this critical level of fluence, the nonlinear refraction in such a material will be dominated by the presence of TPA-generated free carriers. Example values of γ, n_{eh}, and β are provided by Said et al. [38] for ZnSe at an excitation wavelength of 532nm. The result is a relatively low critical fluence on the order of 0.1 mJ cm^{-2}. This indicates that the response of a ZnSe limiter will be dominated by the TPA generation of free carriers rather than the Kerr nonlinearity as was initially proposed. In fact, the responses of most semiconductor limiters that rely on TPA are dominated by self defocusing via free carrier generation [38].

2.4 Induced Scattering

Scattering is a phenomenon that has been of great interest since the study of light and matter interaction was conceived. It is best understood as the radiation that results from light impinging on a material and exciting the material's constituent electric particles. When the oscillations of the incident electric field drive the constituent particles into oscillation, a second electric field is produced. This second field is the radiation known as scattering.

The first analytic description of scattering was presented by Lord Rayleigh in 1899. This form, known as Rayleigh scattering, only applies to particles that are significantly smaller than the wavelength of the excitation. Rayleigh's mathematical description provides a model in which the intensity of the scattered radiation is equal in both the forward and backward directions. However, this model breaks down when the size of the particle approaches around 10% of the wavelength. A more complete model was subsequently introduced by Gustav Mie in 1908. This model, known as Mie scattering, is more complex but capable of handling particle sizes on the order of the excitation wavelength or larger. According to Mie theory, the ratio of scattering in the forward versus backward directions increases with the particle size to wavelength ratio. That is to say that, as the particle size increases, so does the intensity of scattering along the direction of the incident excitation. It can therefore be concluded that scattering from particles sized on the order of the wavelength or greater is an undesired effect in optical limiting since much of the energy will be directed toward that which we wish to protect. Instead, limiter design via scattering focuses on the use of particles that are much smaller than the incoming wavelength.

The concept of induced scattering is key to the utility of scattering in the design of a limiter. Since an ideal limiter is transparent at low intensities, reduced throughput by stationary scattering is undesirable. While several methods of inducing scattering within otherwise linear solids are known, the induction of additional scattering within a solid typically leads to irreversible changes that alter the linear performance. Therefore, induced scattering most commonly takes place in liquids. The simplest method of induction in a liquid is to excite absorbing molecules in solution. The absorbing molecules within the liquid solution take up the incoming energy and heat the

solution until the boiling point is reached. When the liquid boils, small vapor bubbles form from the solution and create scattering centers. The large refractive index discontinuity at the vapor-liquid boundary is responsible for the resultant scattering effect. The caveat to this simple design is that the vapor production process takes as long as nanoseconds or even microseconds [33]. This activation delay renders such a limiter useless for threats on the order of picoseconds or less. However, the bubbling effect remains an effective secondary mechanism for limiting on longer timescales.

A more creative material design is required for the effective limiting of short pulses. One such design involves crystalline filters in colloidal suspension [4]. These filters are composed of index-matched spheres suspended within an ionic liquid. If the spheres are charged and of the same sign, then they will assemble into either a body-centered or face-centered cubic lattice. Under low intensity illumination, no scattering occurs from the spheres due to the matching of their refractive index with that of the solvent. However, refractive index change within the spheres under a strong excitation produces a periodic variation in the refractive index of the solution. This periodic structure effectively becomes a grating that causes the incident illumination to diffract. The greater the strength of the excitation, the greater the index change and, therefore, greater the efficacy of diffraction. The result is energy directed away from the path of incident illumination. Of course, this design has caveats of its own. Of particular significance is the limited applicability in temporal and spatial spectra of the diffraction grating to the incoming threat. The threat must meet the Bragg condition which only occurs for narrow temporal bandwidths and incident angles.

Perhaps an even more creative approach is through the use of stimulated scattering. This method involves the traversing of an incident wave within a medium that contains scattering centers. The backscattered wave beats against the incident wave and sets up a standing density wave inside the medium. This density wave promotes further backscattering of the incident field. As the incident intensity increases, so does the magnitude of the density wave. The result is an even stronger backscatter response. Further enhancement to the energy-diversion ability of such a material is achieved by focusing the incident light with a cylindrical lens and placing mirrors within

the material along the lens's long axis. If the position of the mirrors is within a peak of the density wave, then a cavity is formed and the stimulated emission may exceed its threshold. In this case, lasing can be achieved and substantial amounts of energy are diverted in a direction along the cylindrical lens's axis, perpendicular to that of the illuminating beam. The caveat to this setup is that it requires monochromatic, coherent light – an extremely narrowband case.

2.5 Photorefraction

Despite having been categorized as a form of nonlinear refraction, the action of photorefraction in optical limiting is quite unlike the mechanisms described in Section 2.3. In fact, the devices described here are more similar to those in stimulated scattering in that they rely on interference between multiple waves to create periodic structures of varying refractive index. These are accumulative nonlinearities that depend on the redistribution of charges and are material limited due to their $\chi^{(2)}$ dependency. This requisite anti-symmetry excludes the use of liquids or centrosymmetric crystalline solids in photorefractive limiters [19]. In those materials that do exhibit a $\chi^{(2)}$ response, photorefraction occurs through the optical excitation of deep levels that results in the production of free charge. The excitation of these deep levels is accomplished within peaks of high intensity that are generated by interfering two coherent beams within a material. The free carriers generated at these peaks then diffuse into nearby valleys, creating a spatially varying charge distribution in accordance with the interference pattern of the two beams. In an appropriately oriented non-centrosymmetric crystal, the distribution of charge creates a periodic change in refractive index; this is effectively a grating.

Two devices that utilize the photorefractive effect are the beam fanning limiter and the coherent-beam excisor. These devices are distinguished from one another by the source of the interfering beam. In the beam fanning case, the source is backscatter from crystal imperfections or inclusions in the limiting medium. The scattering from these inhomogeneities interferes with the incident beam and sets up a photorefractive grating. The anti-symmetry of the crystal imposes a preferential direction of energy transfer such that, when properly oriented with respect to the incident

beam, the gratings divert energy to one side of the crystal and away from the optical path. This process has been shown to be effective in constructing an optical limiter by Cronin-Golomb & Yariv [18] despite the inherently slow response of charge transport. Rather than relying on internal scattering, the coherent-beam excisor seeds the photorefractive grating with a weak beam designed to interfere with the incident threat. The crystal and the seed beam are oriented such that, when the input is of high intensity, the induced grating couples energy from the strong incident beam into the weaker seed beam, thus diverting it from the optical path. This method increases the speed of the device response as well as its efficacy in diverting energy away from the sensor [44].

A few key characteristics set the photorefractive optical limiter apart from its peers. The first is the strict dependency on coherent light. This feature has both advantages and disadvantages. The advantage lies in the ability to limit a high intensity coherent threat (e.g. laser) without disrupting the ability of the sensor to detect low intensity incoherent light. This provides a clear means of protection from deliberate threats without rendering the sensor blind to the environment. The disadvantage of this feature is that these devices are ineffective against high intensity incoherent threats such as arc or flash lamps. Another distinguishing characteristic is that the photorefractive index change is independent of the illuminating intensity. Rather, the delay of the redistribution of charges and, therefore, the index change, is the intensity dependent parameter. The implication is that the response time is inversely proportional to the intensity but the efficacy of the response remains independent. Despite this adaptation of the response time to the strength of the input, the inherent delay in distributing charges remains the primary limitation of photorefractive limiting. Such devices are typically ineffective in protection against pulses on the order of nanoseconds or less [44].

Chapter 3

Widely Studied Limiting Materials

Abstract

The majority of limiting research focuses on the development of new materials or the identification of existing materials in which strong nonlinear responses occur. A few of the material classes that have been widely studied are semiconductors, organometallics, carbon black suspensions, fullerenes, and liquid cyrstals. While most of these materials exhibit multiple nonlinear effects, it is typical that one such process dominates the overall optical response. This chapter identifies the optical nonlinearities of those materials and examines their efficacy in optical limiting applications.

3.1 Semiconductors

Semiconductors are a promising class of materials for optical limiting applications due to their wide range of nonlinearities. As discussed in Section 2.3, direct bandgap semiconductors exhibit a strong nonlinear response at energies near the band edge. Due to the narrow bandwidth of this response and its tendency to saturate, however, this effect of seemingly significant opportunity has not been extensively used in limiting devices. The nonlinearities that have received more attention in this area are free-carrier absorption, two-photon absorption, nonlinear refraction due to the Kerr effect, and nonlinear refraction associated with free-carrier generation. Optical limiting in semiconductors was first demonstrated by Geusic et al. [21] in the 1960's via nonlinear absorption. In 1984, silicon (Si) was used to construct a device in which nonlinear refraction was shown to be a significant contributor to the limiting action at 1.06μm [12]. Gallium arsenide (GaAs) was shown

to produce similar results to Si during picosecond excitations of the same wavelength the following year [9]. This is particularly interesting given the considerable differences in the underlying nonlinear mechanisms of the two materials. Discussion of the similarities and how their behaviors diverge with increasing timescales is offered in this section along with other semiconductors of interest to optical limiting.

3.1.1 Silicon

Silicon is an indirect bandgap material with a bandgap energy of 1.1eV at room temperature. The aforementioned 1.06μm (1.17eV) excitation is sufficient to couple the peak of the valence band with X-valley minima in the conduction band. This linear, phonon-assisted absorption generates free carriers which are then available to absorb additional photons. Hence, the nonlinear free-carrier absorption limiting mechanism. Of even greater significance in the interest of limiting is the reduction of the refractive index by the presence of the generated free carriers, the details of which are described by a Drude model [44]. This change in index in accordance with the beam profile produces a negative lens that defocuses the beam as shown in Fig. 2.2a. The subsequent reduction in transmitted intensity is significantly greater than that induced by the Kerr effect or free-carrier absorption alone.

We recall from 2.2.2 that TPA is intensity dependent and, therefore, effective only for short pulses. Additionally, we can ignore diffusion and recombination effects in pulses that are shorter than their respective timescales. TPA responses can be neglected for pulses in excess of 10ps while diffusion and recombination effects are on the order of 100ns for a spot size $\sim$10μm [44]. It is within this range of pulse widths that the limiting behavior of Si can be fully described by the linear absorption coefficient, α, the free-carrier absorption cross-section, σ, and the change in index per carrier pair, n_{eh}. The nonlinearities are then dependent only on carrier density and, since the free carriers are generated through linear absorption, are strictly fluence dependent. That is to say that the nonlinear response of silicon under the specified range of pulse lengths is independent of the incident pulse duration. Therefore, the behavior of Si-based limiting devices is also

independent of pulse duration for excitation timescales on the order of picoseconds to hundreds of nanoseconds. Boggess et al. [11] determined that the limiting response of Si can be described by $\sigma = 5 \times 10^{-18}\text{cm}^2$ and $n_{eh} = -10^{-21}\text{cm}^3$ for 25ps pulses at 1.06μm. Since the effective masses of the affected carriers are relatively large, an abundant density of states occurs in both bands. This allows substantial carrier densities to be generated, on the order of 10^{-19}cm^{-3} for fluences $\sim$200mJ cm^{-2}, without saturation. These high carrier densities and observed n_{eh} combine in Equation (2.13) to produce significant changes in refractive index, $\Delta n \sim 0.01$. The result is ample defocusing and, thus, an effective limiter.

Silicon appears to be an exceptional candidate for a limiting material in micron wavelengths. It exhibits strong nonlinear refraction, maintains a consistent response across a wide range of pulse widths, and is void of saturation effects and resistant to thermal damage when exposed to large fluences. However, the semiconductor falls short as a limiter when the threat is wideband. The bandwidth of the limiting response is constrained due to the resonant nature of carrier generation in Si. Its ability to perform as an ideal limiter is further restricted by the frequency dependence of the linear absorption coefficient. Silicon only performs as both an ideally transparent (linear) material and an adequate optical limiter across a narrow range of bandwidth.

3.1.2 Gallium Arsenide

Gallium Arsenide differs from silicon in that it is a direct bandgap material with a 29% larger gap. The room temperature bandgap of GaAs is 1.42eV. This is far too large for the excitation of charges from the valence band to the conduction band by single 1.06μm photons. However, significant absorption and subsequent carrier generation are possible through TPA. This nonlinear absorption reduces transmission in short pulses, but of greater significance is the resulting nonlinear refraction. The change in index is a consequence of accumulating carrier densities and the instantaneous response of the Kerr effect. Both nonlinear mechanisms are well described in GaAs by their respective models, (2.17) and (2.16) [44].

The limiting response of gallium arsenide is unlike that of silicon due to its dependence on

intensity rather than fluence. This is due to the differing mechanisms of absorption and resultant carrier generation. GaAs depends on TPA, a duration-sensitive absorptive mechanism, whereas Si relies on linear absorption that is duration independent. This TPA dependency is multi-faceted; it is responsible for the fast-acting short-pulse absorption and instantaneous nonlinear refraction as well as the accumulating changes in refractive index. Such relationships with intensity are what set the GaAs limiter apart from the pulse-duration independent Si model.

Boggess et al. [9] have determined that the TPA coefficient of gallium arsenide is $\sim$25cm GW^{-1} and the free carrier cross section is $\sim 3 \times 10^{-18}$cm^2. Meanwhile, Said et al. [38] have demonstrated that the coefficient that relates the change in refractive index to the input intensity as a consequence of the Kerr effect is $\gamma = -3.3 \times 10^{-4}$cm^2 GW^{-1} and the change in index per photogenerated carrier pair is $n_{eh} = -8 \times 10^{-12}$cm^3. These parameters have all been determined for excitations at 1.06 μm and, therefore, completely describe the limiting behavior of GaAs for near micron wavelengths. It can be shown by insertion of these values into their respective models that GaAs is only effective as a limiter for short, subnanosecond pulses [44]. This is a direct consequence of reliance on the TPA nonlinearity, which is itself a consequence of the semiconductor's wider bandgap. In fact, the TPA coefficient is even smaller in materials with bandgaps greater than gallium arsenide's [43]. This leads to the conclusion that other large gap semiconductors that could be considered for limiting at visible wavelengths may only be effective for short pulses as well. There remains a trade-off, though, between TPA limiters and those that depend on linear, single-photon absorption. The frequency dependence of the TPA coefficient is significantly weaker than that of linear absorption [46]. Thus, semiconductor limiters whose primary action is TPA are far less restricted in operational bandwidth than those that rely on a linear process.

Despite the notable differences in timescale-dependent behavior, the limiting transmissivity of Si and GaAs are remarkably similar for picosecond excitations. Figure 3.1 [44] displays the transmitted energy per incident fluence of Si and GaAs for 25ps pulses at 1.06μm. The represented experiment consisted of a 3mm thick sample of GaAs and a 1mm thick sample of Si, each placed near an intermediate focal plane of an f/250 optical system to ensure activation of nonlinear mech-

anisms. Both materials exhibit strong limiting behaviors under fluences as low as 20mJ/cm^2 and clamp the total output energy at around 100nJ. It is within these ascribed parameters that both materials perform equally well as optical limiters. Beyond the limitation of subnanosecond excitations, the behavior of GaAs degrades and diverges from the duration independent response of silicon.

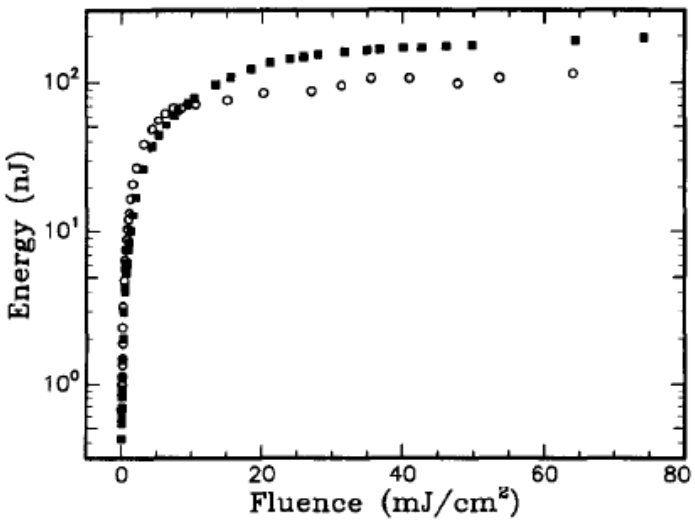

Figure 3.1: Limiting response of Si (solid squares) and GaAs (empty circles) for 25ps pulses at 1.06μm [44]

3.1.3 Large Bandgap Semiconductors – Visible Wavelengths

The variety of nonlinear mechanisms within silicon and gallium arsenide have been studied extensively for their applications to optical limiting. However, despite their efficacy in constraining threats at near-micron wavelengths, the relatively small bandgaps of these two materials render them ineffective against threats in the visible realm. It is for this reason that interest has been generated in larger bandgap semiconductors. Two noteworthy examples are GaP and ZnSe. GaP, an indirect bandgap material with a gap of 2.27eV, is analogous to Si in the limiting sense. Excitations near the band edge (e.g. green laser at 532nm = 2.34eV) result in phonon-assisted linear absorption that produces free carriers in the X-valley minima of the conduction band. The presence

of these free carriers leads to free-carrier absorption as well as nonlinear refraction, the latter of which dominates the limiting response. This description mimics that of silicon in 3.1.1. GaP and Si differ in the significance of the interband contributions to the change in index. This is due to the presence of a direct bandgap at only 0.51eV above the indirect gap in GaP while the smallest direct bandgap in Si is 2.4eV away. Thus, the interband contribution in GaP is significant at 532nm while it is insignificant in Si at 1.06μm. Large populations of free carriers are attainable in GaP thanks to the long recombination times of the indirect bandgap and the high density of states in the valence and conduction bands. Like silicon, the resulting index change is the primary form of limiting action. It has been reported that limiting at levels acceptable for human eye protection is possible in this material for 25ps pulses [37]. Deduction through the similarities to Si suggests that GaP should perform similarly for threats on the nanosecond timescale as well. However, this also suggests the same limitation of narrow bandwidth applicability.

Where GaP is similar in optical limiting to Si, ZnSe is a visible wavelength equivalent to GaAs. Also a direct bandgap semiconductor, ZnSe has a room-temperature bandgap of 2.67eV. This large bandgap renders the material transparent to low intensity excitations over most of the visible spectrum. However, significant TPA occurs for high intensity illumination at 532nm. The TPA coefficient at this wavelength is 5.5cm GW^{-1} and the index change per carrier pair is -8×10^{-20}cm^3 [38]. While these values are many orders of magnitude smaller than those of GaAs, the ZnSe exhibits similar behavior to the near-infrared limiting material. Both have the potential for limiting broadband excitations but are only effective for short pulses due to the small TPA coefficients.

The presented examples demonstrate the abundance of nonlinear mechanisms available in semiconductors for optical limiting. Silicon and gallium arsenide prove to be strong candidates for limiting of short, narrowband pulses. Si extends into longer pulse widths but only for narrow bandwidths while GaAs is constrained to short pulses but capable of handling wider bandwidths. GaP and ZnSe are shown exhibit similar nonlinear characteristics to their longer wavelength counterparts, though we see through the empirically derived coefficients that ZnSe has a weaker re-

sponse. These tradeoffs illustrate the conundrum of semiconductor-based optical limiter design. While each material offers many properties of interest, no single semiconductor provides all of the desired traits of an ideal limiting device.

3.2 Organometallics

Organic materials are of interest in optical limiting because many of them have been shown to exhibit reverse saturable absorption. In fact, RSA was first observed in 1967 via organic compounds [22]. Organometallics resemble organic compounds but include at least one metal. The inclusion of a metal adds optical transitions that would not otherwise occur. Such transitions may occur between the d orbitals of the metal, d–d electronic transitions, or between the organic ligands and the metal. The metal-to-ligand charge transfer (MLCT) transitions occur when an electronic from the metal is donated to the ligand. Conversely, the ligand-to-metal charge transfer (LMCT) transitions occur when an electron from the ligand is donated to the metal. Intraligand transitions in which the optical absorption occurs completely within the organic portion of the compound are also possible. Since charge transfer transitions result in a separation of charge, they couple well to applied electric fields and yield high extinction coefficients [44].

3.2.1 Metal Macrocycles

There are two primary categories of organometallics that have been studied in regards to optical limiting. They are metal macrocycles and metal cluster compounds. Of the macrocycles, metal phthalocyanines and naphthalocyanines have been of particular focus. These compounds are typically strong absorbers in bands on either side of the visible spectrum—a Soret band in the ultraviolet and a Q band in the red to infrared. Absorption in the visible spectrum is weak and has little frequency dependence which is preferable for the ground state of an RSA material. An example of such a macrocycle is chloroaluminum phthalocyanine (CAP). CAP exhibits substantial excited state absorption that is dominated by singlet–singlet transitions for short, subnanosecond pulses.

Under longer excitations, triplet–triplet transitions become the dominant effect [17]. It is due to this evolution of absorptive mechanisms that CAP demonstrates pulse-length and frequency dependent limiting capabilities. Researchers have estimated that the excited-state absorption cross section is 10–50 times larger than that of the ground state at 532nm. While this is substantial enough for effective RSA action, there is a caveat nearby. The Soret band is located at 670nm, causing the material to behave like a saturable absorber in the visible spectrum [28]. This is the opposite of the desired RSA response. Thus, the applicable bandwidth of CAP in an optical limiter is in the green-to-blue region of the spectrum. Silicon naphthalocyanine (SINC) does not have this limitation. This macrocycle was shown to have a high third order susceptibility at 1.907μm [45] and its Q band lies outside the visible spectrum at 778nm. With a substantially lower limiting threshold [36] and a limiting response that spans the entire visible spectrum, SINC promises to be an effective RSA material for use in these applications.

Other organometallic macrocycles have been reported to possess limiting properties. RSA has been demonstrated in free tetraphenyl porphyrins (H2TPP) and in metallated ZnTPP and CoTPP [7]. It was deduced that RSA in the zinc compound occurred through singlet–singlet absorption and that the cobalt compound underwent triplet transitions during 80ps excitations. Additional work has shown that FeTPP also exhibits RSA behavior and a large χ^3 [44]. It seems that many combinations of metals and organic macrocycles present opportunities for application in limiting via RSA.

3.2.2 Metal Cluster Compounds

Metal cluster compounds are organometallics that contain two or more multiply interbonded metals whose valence shells are completed by the ligands. Typically, the least energetic transition is from a bonding d orbital shared by the metals to an antibonding d orbital within the core. These absorptions in the visible spectrum are typically with extinction coefficients of 10–10,000 M^{-1} cm^{-1}. Tutt & Boggess [44] hypothesized that excited state absorption in these compounds would occur due to a charge transfer transition, having typical extinction coefficients of 1000–300,000 M^{-1} cm^{-1},

and that this would result in RSA behavior. Their hypothesis was confirmed through the examination of iron–tricobalt cluster compounds in which they demonstrated that the excited state absorption involves the ligand directly. Upon exchanging organic solutions, the ground state absorption was unaffected while the optical limiting properties were significantly altered. This experiment was instructive in identifying the components of the material that contribute to its RSA properties. However, due to the air sensitivity and photodecomposition dependent absorption cross-section, this particular material is regarded as impractical for limiting device construction.

Another compound, known as King's complex or $(Fe(CO)_4Cyclopentadienyl)_4$, has been studied for its limiting properties by Allan et al. [1]. This metal cluster remains extremely stable when exposed to heat, light, and oxygen, and is thus a more practical solution for physically realizable devices. The investigators observed limiting from solutions of King's complex in toluene and methylene chloride. Under picosecond excitations, they were able to determine absorption cross-sections for both the ground (σ_1) and excited (σ_2) states as well as lifetimes τ_2, τ_3, and τ_{24}. However, these parameters when fitted to a five-level model did not agree with the response of the material under nanosecond excitations. Further investigation revealed significant off-axis nonlinear scattering. The authors compensated for this effect by incorporating the compound into a solid host polymethylmethacrylate (PMMA). The induced scattering from King's complex was eliminated and it was found that the three-level model of singlet states accurately described the nanosecond response. Since little-to-no contribution from triplet state transitions was required, it was determined that the majority of limiting in nanosecond pulses by King's complex is due to induced scattering with a small contribution by RSA from excited singlet absorption [10].

A variety of compounds that exhibit RSA behavior were examined under 532nm nanosecond excitations for comparison as shown in Figure 3.2. It should be noted that these responses are a combination of RSA and scattering, since it has been determined that induced scattering dominates the King's complex under these conditions. The effects of RSA and scattering are inseparable in this experiment so these limiting thresholds may be considered an upper limit for the RSA abilities of each compound. Tutt & Boggess [44] point out that the range of these thresholds varies by a

maximum factor of ~20 and states that "Because of their widely varying optical properties and the potential for molecular engineering to allow tailoring of a molecule to a specific application, organometallic compounds are very attractive for optical limiting." However, the many orders of magnitude discrepancy between this range and the requirement for direct human eye protection is suggested to be too great for closure.

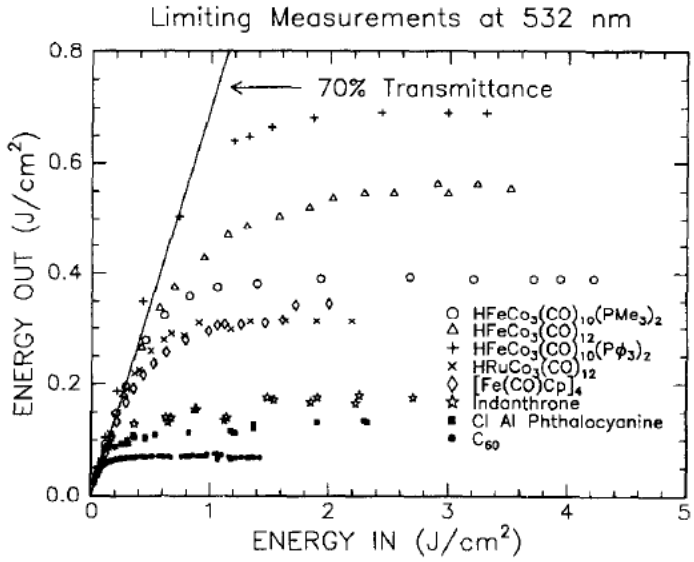

Figure 3.2: Limiting response of various RSA materials at 532nm [44]

3.3 Carbon Black Suspensions

Carbon is known to be a nearly uniform absorber for wavelengths in the visible spectrum, hence its dark and colorless appearance. When small, subwavelength particles of carbon are suspended in a liquid they comprise a material known as carbon black suspensions (CBS). It was first demonstrated in 1991 at a Department of Defense Workshop that limiting action occurs when CBS is exposed to high intensities. Further studies have shown that while this limiting behavior is a consequence of several nonlinear mechanisms, one is dominant [33, 35]. The observed mechanisms include nonlinear absorption, nonlinear scattering, and nonlinear refraction. We will see that induced scattering is the dominant effect in limiting by CBS solutions.

These colloidal solutions of carbon and typically alcohol are filtered such that the suspended particles remain smaller than the wavelength of incident light ($< 0.5\mu$m for visible). The motive for this constraint on particle size is twofold. Since linear scattering from such small particles is insignificant, this prevents substantial distortion and attenuation of the low intensity image. This restriction also prevents precipitation of the carbon thanks to sufficient Brownian motion [44].

The CBS reaction to high intensity illumination is understood as follows: the carbon particles absorb the visible light which causes the particles to break apart and also heats the surrounding liquid. Under sufficient intensity, a white flash has been observed to emit from the solution. This flash has a spectrum corresponding to blackbody radiation around 4500K and a lifetime of $\sim$30ns when the excitation is comparably shorter. The formation of microplasma is consistent with these observations, suggesting that the phenomenon is occurring within the solution in response to excitation. Despite the apparent initial absorption effects, it has been shown that the dominant mechanism becomes induced scattering for longer timescales [30]. This work also detected a weak nonlinear refraction effect but indicates the primary limiting mechanism in CBS for nanosecond timescales is the induced scattering that results from microplasma formation. Under longer excitations, the liquid eventually boils and the bubbles contribute additionally to the scattering response.

As with any material, carbon black suspensions have both advantages and downfalls in limiting applications. Carbon's absorption spectra is flat for visible wavelengths and therefore renders CBS effective across a wide band of excitations. The dynamic range of this limiter has the potential to be large considering that the scattering results from carbon break-up which can reaggregate or be replenished by new material. Since CBS is a liquid medium it can self-heal as well. Caveats are that limiting material is displaced from the interacting volume, rendering the solution less effective for repeated pulses, and that agglomerations and precipitation of carbon have been observed after subsequent pulses. The first of these can be mitigated by continued agitation and recycling of the solution while the latter may be disregarded as the cost of periodic replacement is small.

3.4 Fullerenes

Buckminster fullerenes (buckyballs) are a class of compounds that grew in popularity after the publication of their simple synthesis in 1990. These highly symmetric carbon cage-structure molecules exhibit a variety of interesting properties including but not limited to higher temperature superconductivity, resistance to deformation, the ability to reversibly accept 6 or more electrons, and the capacity to trap atoms within [44]. The excitement behind these unique properties led to investigation of the optical response of fullerene molecules which has been largely focused on the quantification of optical transitions. Early research discovered that the excited state absorption cross section of the C_{60} molecule is greater than that of its ground state for the entire visible spectrum [2]. Thus, this material exhibits RSA properties and may be suitable for optical limiting in the visible regime. It was determined by scientists at Hughes Research Laboratories (HRL) that the absorption cross section for C_{60} in toluene solution does not vary by more than a factor of 2 for wavelengths from 425nm to 625nm [44]. The excited state absorption was measured by Sension et al. [40] and maintains the same general trend as the ground state absorption. These observations reveal that the fullerene should exhibit near ideal characteristics as a RSA based optical limiting material in the visible range. The experiments at HRL also investigated C_{70} and found that its absorption spectra experiences a shoulder at 590nm with increasing absorbance as the wavelengths shorten. This response is less desirable as the larger ground state absorption reduces the effectiveness of RSA action.

HRL designed their experiment such that the Rayleigh length of the excitation at the sample was long with respect to the sample thickness. This resulted in a near constant spatial profile of the beam throughout the sample, thereby reducing the effects of nonlinear refraction and rendering the transmission particularly sensitive to nonlinear absorption and scattering. When this experiment was performed on C_{70} at 532nm, it was found to perform as an effective limiter but at a much higher limiting level than C_{60}. The C_{60} fullerene in a 63% transmitting sample clamped the output at a fluence of $\sim$60mJ cm^{-2} under the 8ns excitation. With the five level model parameters for C_{60} determined from prior publications, it was observed that the expected limiting level was about

twice that of HRL's experimental results. This suggested that other nonlinear mechanisms were responsible for the limiting action of the carbon compound. Off-axis scattering was measured and found to vary nonlinearly with the incident intensity, indicating that nonlinear scattering is likely responsible for the remainder of the limiting action since nonlinear refraction was minimized via the experimental arrangement. Symmetry was observed between forward and backward scattering which leads to the conclusion that the scattering centers may be well described as Rayleigh scatterers that are smaller than the excitation wavelength.

Further investigation of the nonlinear mechanisms of C_{60} was performed by embedding the fullerene in a solid host, polymethylmethacrylate, at similar concentrations to those of the toluene solutions [27]. The absorption spectrum was nearly identical to the solution's, indicating that the electronic states were essentially unchanged. Scattering from the material was observed to be linear until breakdown of the host at $\sim$1200mJ cm^{-2}. This allows for a simple correction of the scattering since its nonlinear nature as observed in solution was defeated. Significantly higher limiting levels were observed in the solid host and the five level model was found to predict this behavior accurately. Therefore, the limiting action of C_{60} in a solid host can be completely described by nonlinear absorption and it is concluded that the response of the liquid solution combines this behavior with nonlinear scattering in similar strengths.

Additional research was performed on the C_{60} & C_{70} compounds in toluene solution by Brandelik et al. [13] in a converging beam configuration. Their experiment was employed by a focusing lens that tightened the beam to a very small region of high intensity within the sample. This arrangement allows for the examination of nonlinear refraction within the material as well as separating it from the nonlinear absorption and nonlinear scattering via the Z-scan technique. Nonlinear absorption is reduced as a consequence of the smaller region in which high intensity occurs via this method. The results demonstrated a limiting threshold of 330mJ cm^{-2} in a 66% transmitting sample and 19mJ cm^{-2} in a 34% transmitting sample. Variations in the intensity versus transmitted angle were shown to be consistent with thermal defocusing and the Z-scan results suggested strong nonlinear refraction that is consistent with thermal lensing. These observations reinforce the five

level model in which the radiationless intersystem crossing from the excited state to the triplet state results in a loss of about 30% of the 532nm energy [44]. This loss is dissipated thermally, hence the thermal lensing effects. The Z-scan also revealed a strong nonlinear absorption component at sufficiently high fluences. This is consistent with the aforementioned findings of HRL.

The presence of several nonlinear mechanisms at significant strengths in these compounds affirm the assertion that fullerenes present a promising material for use in optical limiters. While their inclusion in a solid host allows for precise prediction of the limiting threshold, they are most effective in solution where multiple mechanisms can contribute simultaneously. The configuration dependence provides an additional degree of freedom in choosing the precise device behavior. Overall, buckyballs are an appropriate choice of medium for a diverse set of limiting applications in the visible regime.

3.5 Liquid Crystals

Liquid crystals are well known for their applications as active devices in which applied electric fields orient the anisotropic molecules to generate visual displays. As with any active, feedback reliant device, the delay between excitement and response is large compared to durations of modern laser pulses. While the active mode may be impractical for optical limiting applications, researchers have shown that these ordered liquid materials possess properties useful for passive limiters.

The nematic phase is the most commonly used mesophase of liquid crystals. It maintains fluidity similar to an ordinary isotropic liquid but the molecules arrange in a long-range order, their long axes aligned parallel with one another. These rod-shaped molecules are easily oriented by applied electric or magnetic fields and exhibit optical properties of uniaxial crystals under such conditions. Nematics have also been shown to be particularly useful in limiting applications due to some unique properties. Their geometric anisotropy solicits largely differing responses along the ordinary and extraordinary axes. This polarization dependence results in substantial birefringence while the material remains transparent [26]. Temporally, nematic liquid crystals exhibit several

distinct nonlinear responses. Two of these trends occur as nonlinear variation in refractive index. The fast response occurs in about 100ns while the slower of the two peaks in 10ms [25]. Self diffraction of the incoming beam has been observed on even shorter timescales as well.

Though not as thoroughly featured as the nematic phase, isotropic phases have been shown to exhibit two photon absorption as large as $\sim$0.6cm GW^{-1} [42]. The drawback is that these linear crystals exhibited nonlinear refractive indices an order of magnitude smaller than studied nematic crystals. Despite the diminished self-lensing effect, the combination of TPA and nonlinear refraction in isotropic phase liquid crystals has successfully limited 30ps, 532nm pulses at thresholds as low as 0.15μJ.

Liquid crystals alone have not proven to be as fruitful as some of the aforementioned materials in passive limiting devices. The slow variation in nonlinear refractive index renders the nematic phase ineffective against threats on nanosecond and shorter timescales while the fast-acting TPA response of the isotropic phase is less effective against longer pulses. However, liquid crystals may prove to be an effective addition to limiting devices when used in concert with materials whose properties complement their weaknesses. In example, active feedback-driven limiting devices may be implemented via liquid crystals to protect against longer threats while paired with fast-acting passive devices. The possible combinations are plentiful and, thus, liquid crystals remain a valuable tool in the kit of optical limiter design.

Chapter 4

Parametric Resonances in Plasmonic Nanoparticles

Abstract

A newly developed category of metamaterials exploits the classical concept of parametric resonance for indirect transfer of energy by an external source. This phenomenon, known as plasmonic parametric resonance (PPR), increases the energy of a system by modulating the characteristic eigenfrequency of plasmonic modes at optimal phases of evolution between states of potential and kinetic energy. The targeted plasmonic modes exist in mixed media that are composed of metallic nanoparticles embedded within a dielectric background. Particularly significant is the ability of PPR to deliver energy from a spatially uniform pump to arbitrarily high order modes. This enables an incoming threat to access an infinitely dense set of discrete modes within subwavelength particles that appear otherwise transparent below a threshold intensity. Thus, the door is opened for these PPR materials to operate as plasmonic parametric absorbers (PPA) and contribute to the field of optical limiting. This chapter introduces the fundamentals of PPR and exemplifies the use of PPA materials in optical limiting applications.

4.1 Localized Surface Plasmons

Localized surface-plasmon (LSP) resonances are a salient feature of the optical and electronic response of metallic nanoparticles. These modes can be externally excited by photonic or electronic scattering, leading to strongly localized electric fields in proximity of the nanoparticle's surfaces. An enhanced optical response is obtained when LSPs are resonantly excited by an incident field

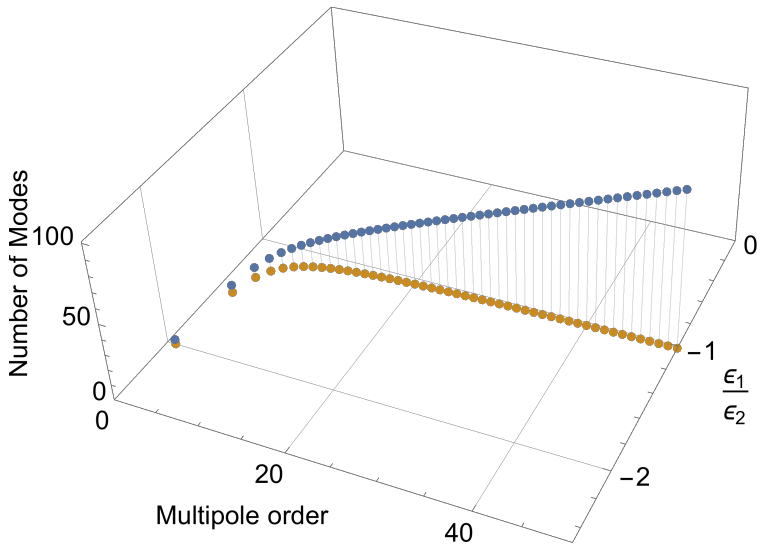

Figure 4.1: Spectral distribution of the LSP resonances in a plasmonic sphere

at the characteristic frequency of the dipolar eigenmode. The dynamics of these non-propagating coherent electronic oscillations show a strong dependence on the geometry of the particles, their composition, and the dielectric environment in which they are located. Yet some features are common to all plasmonic configurations. In particular, LSP resonances in nanoparticles of any shape form an infinite discrete set of modes. In the simple case of particles of spherical shape with permittivity $\varepsilon_1(\omega)$ surrounded by a medium with permittivity ε_2, for a resonance of any order n, there are *2n+1* degenerate states with complex frequency ω_n such that $\varepsilon_1(\omega_n) = -(1+n)\varepsilon_2/n$. As shown in Fig. 4.1, for $n \gg 1$, the eigenmodes tend to occur for $\varepsilon_1(\omega_{n\gg 1}) \sim -\varepsilon_2$. The increased modal density for $\varepsilon_1 \sim -\varepsilon_2$ is a general feature of all plasmonic structures. Such increased modal density in plasmonic particles of different shapes for $\varepsilon_1 \sim -\varepsilon_2$ arises because the spatial oscillation of the fields along the particle's surface occurs with a negligible local wavelength compared with the local radius of curvature of the metal-dielectric interface [15]. Accessing such spectrally dense sets of tightly bound resonant modes would greatly enhance nonlinear light-matter interactions at the nanoscale and foster new developments in nonlinear plasmonics [24].

The efficiency with which LSP resonances can be excited by an external incident field depends upon the spatial and spectral overlap between the excitation field and the specific plasmonic mode. For deeply subwavelength plasmonic particles, only the lowest order mode of an electric dipolar

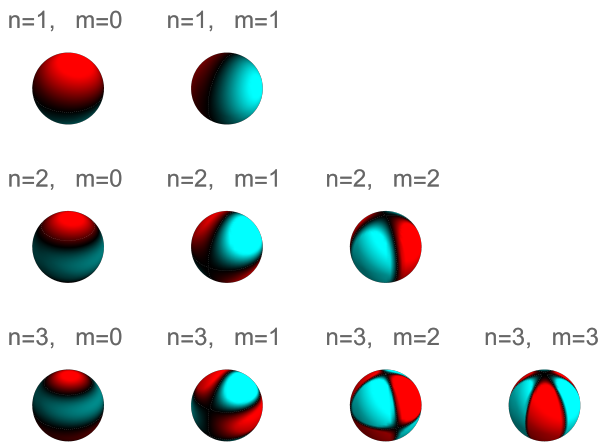

Figure 4.2: Polarization-charge density of the first few resonant modes of a plasmonic sphere

nature is efficiently coupled to radiation states. In order for a particular mode to be efficiently excited, it is necessary for the incident field to be able to induce the appropriate polarization charge distribution. Such polarization-charge distributions are illustrated in Fig. 4.2 for the first few modes of a sphere. From Fig. 4.2, it is apparent that to induce modes of order $n > 1$ the incident field would have to display strong spatial variations over deeply subwavelength regions. That is why the higher order eigenmodes tend to be sub-radiant, and by reciprocity, they are nearly decoupled from free-space propagating fields. Therefore, exciting and detecting such higher-order modes requires either near-field scattering techniques [49] or the use of active media to promote surface plasmon amplification by stimulated emission of radiation (SPASER)[6].

4.2 Plasmonic Parametric Resonance

A different mechanism to drive high-order LSP modes with a spatially uniform optical field relies on the recently introduced concept of plasmonic parametric resonance (PPR)[39]. In contrast with conventional localized plasmonic resonances, in which modes are excited directly by an external field of frequency and spatial profile matching those of a given mode of the plasmonic particle, PPR is a form of amplification in which a pump field transfers energy to a mode indirectly. In PPR, in fact, the modes of a plasmonic structure are amplified by means of a temporal modulation

of the background permittivity caused by an appropriate pump field. Such permittivity variation translates into a modulation of the modal resonant frequency. Under specific pump conditions, amplification can occur. As shown in Ref. [39], among the unique characteristics of PPR is the possibility of accessing modes of arbitrarily high order with a simple, spatially uniform pump, provided that such pump exceeds a certain intensity threshold—a characteristic of all parametric resonances.

In very general terms, a parametric resonance occurs when one or more of the parameters controlling the evolution of a dynamical system undergo a temporal modulation of appropriate amplitude and frequency [14]. When such conditions are met, the amplitude of the parametrically resonant mode increases exponentially with time for as long as the parametric modulation continues. In formal terms, the temporal evolution of a representative dynamical variable *X(t)* of a system with resonant frequency ω_0 and damping γ under the action of a stimulus *F(t)* is given by Eq. (4.1) in the case of direct excitation, and by Eq. (4.2) for parametric excitation.

$$\frac{d^2X(t)}{dt^2} + \gamma\frac{dX(t)}{dt} + \omega_0^2 X(t) = F(t) \tag{4.1}$$

$$\frac{d^2X(t)}{dt^2} + \gamma\frac{dX(t)}{dt} + \left\{\omega_0^2 + 2\omega_0\delta\omega\left[F(t)\right]\right\}X(t) = 0 \tag{4.2}$$

In the parametric Eq. (4.2), the external stimulus *F(t)* acts indirectly on the system by modifying the instantaneous resonant frequency by the amount $\delta\omega\left[F(t)\right]$.

A simple system described by Eq. (4.1) could be a simple harmonic oscillator, like a mass m attached to a spring with elastic constant $k = m\omega_0^2$. In this example, *X(t)* represents the displacement of the mass from the equilibrium position. The restoring force provided by the spring can be described in terms of a potential energy $U = kX^2/2$. As illustrated in Fig. 4.3(a), the free evolution of the system is a damped harmonic oscillation. Now, let us assume that the elastic constant of the spring is changed in time through some external mechanism. This new situation can be effectively described by Eq. (4.2). In the presence of such parametric modulation, the potential landscape varies in time, as shown in Figs. 4.3(b)–4.3(d) for the case of a sinusoidal modulation around the

unperturbed potential. Under the appropriate conditions, the energy that is externally provided to change the potential of the system can be transferred to the harmonic oscillator to compensate for or even overcome the dissipation mechanisms. If a certain parametric modulation threshold is exceeded, the oscillation amplitude grows in time with an exponential envelope as indicated in Fig 4.3(d). In PPR, these concepts are extended and applied to heavily multimode optical resonators such as plasmonic particles.

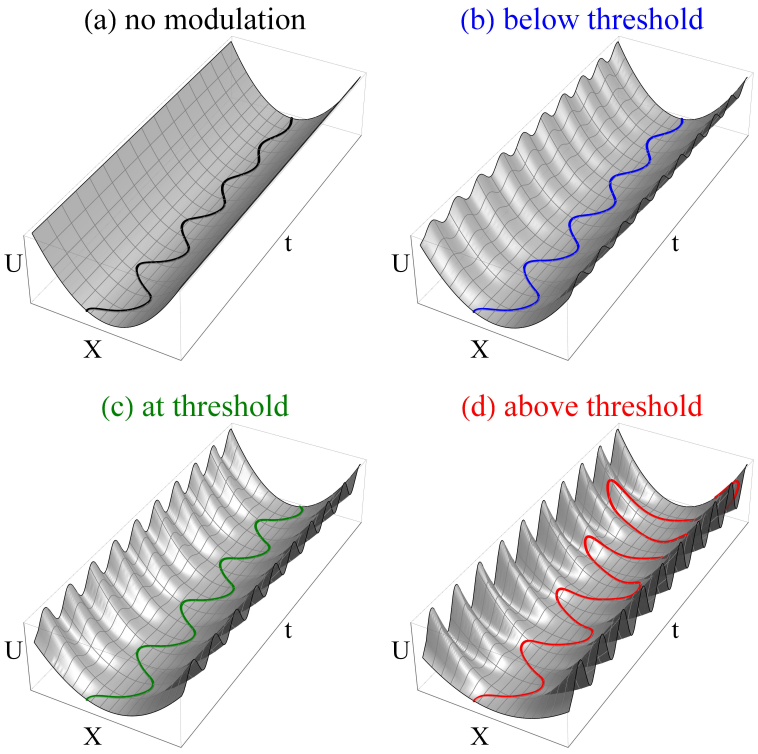

Figure 4.3: (a) Time evolution of the position X of a harmonic oscillator in a parabolic potential U. (b)–(d) Time evolution of a parametrically driven oscillator with time-varying potential. Below threshold (b), the oscillation decays. At the threshold of parametric regeneration (c), the dissipations are exactly compensated. Above threshold (d), the parametric gain causes the oscillations to grow exponentially.

In order to illustrate in general terms the principle of the operation of PPR in a plasmonic nanoparticle of arbitrary shape, the first step is to identify a dynamical variable obeying an evolution equation similar to Eq. (4.2). The first complication that arises is due to the fact that all the relevant physical quantities involved in such an electromagnetic problem are fields of some sort (like electric potential, electric field, magnetic field, polarization density, current density, etc.),

rather than simple kinematic variables like the position *X(t)* considered in the previous harmonic oscillator example. This issue is addressed by performing a modal decomposition of the field of interest in terms of an appropriate complete and orthogonal set of basis functions. By doing so, the field is expressed as a sum of vector-field basis functions, each weighted with a scalar time-dependent modal amplitude determined by the initial conditions and by the subsequent evolution. As shown in the following, such modal amplitudes can be used as dynamical variables to cast the PPR problem in the form of Eq. (4.2). Each modal amplitude will evolve in time, according to an equation of the same form as Eq. (4.1), with an appropriate natural frequency ω_n that depends on the specific mode, the permittivity ε_1 of the particle, and the permittivity ε_2 of the surrounding medium. This approach immediately suggests that modulating one of these properties, say ε_2, will cast the problem in the desired form of Eq. (4.2). In the following, for the purpose of illustration of PPR, we will consider a system that is amenable to a closed-form solution: a subwavelength plasmonic sphere in a homogeneous dielectric background medium.

We consider a sphere of radius R and relative permittivity ε_1 (medium 1) embedded in a uniform dielectric medium ε_2 (medium 2). The radius R is assumed to be much smaller than the free-space wavelength associated with any of the plasmonic eigenmodes of interest, so that a quasi-static approach is applicable for determining the spatial distribution of the electromagnetic field. The dispersion of ε_2 is neglected. Medium 1 is assumed to follow a Drude-like frequency domain dispersion $\varepsilon_1 = \varepsilon_\infty - \omega_{pl}^2/(\omega^2 + i\omega\gamma)$, with plasma frequency ω_{pl}, collision frequency γ, and a non-dispersive term accounting for high-frequency spectral features ε_∞. The dispersive term in the $\varepsilon_1(\omega)$ expression is associated with the equation of motion for the free-carrier polarization density $\mathbf{P}_1(\mathbf{r}, t)$ within medium 1 where $\mathbf{E}_1(\mathbf{r},t)$ is the electric field:

$$\frac{\partial^2 \mathbf{P}_1(\mathbf{r},t)}{\partial t^2} + \gamma \frac{\partial \mathbf{P}_1(\mathbf{r},t)}{\partial t} = \varepsilon_0 \omega_{pl}^2 \mathbf{E}_1(\mathbf{r},t) \tag{4.3}$$

Within the quasi-static approximation, the potential of an electric multipole eigenmode of order (*n,m*) can be expressed in terms of even and odd spherical harmonics, $Y_{n,m}^{(e,o)}(\theta,\phi)$. It is under

this assumption that the polarization density in medium 1 can be expanded in terms of spherical harmonics with time-varying coefficients $\mathbf{P}_{n,m}^{(e,o)}(t)$, defined and normalized as in Ref. [39]:

$$\mathbf{P}_1(\mathbf{r},t) = \sum_{n,m} \nabla \left\{ \frac{\mathbf{r}^n}{R^{n-1}} \left[\mathbf{P}_{n,m}^{(e)}(t) Y_{n,m}^{(e)}(\theta,\phi) + \mathbf{P}_{n,m}^{(o)}(t) Y_{n,m}^{(o)}(\theta,\phi) \right] \right\} \tag{4.4}$$

Thanks to the orthogonality of spherical harmonics, the electromagnetic boundary conditions are applied at $r = R$ to yield to separate equations of motion for the polarization density amplitudes $P_{n,m}^{(e,o)}(t)$ of each angular momentum state,

$$\frac{d^2\mathbf{P}_{n,m}^{(e,o)}(t)}{dt^2} + \gamma \frac{d\mathbf{P}_{n,m}^{(e,o)}(t)}{dt} + \omega_n^2 \mathbf{P}_{n,m}^{(e,o)}(t) = 0, \tag{4.5}$$

where modal radiation effects have been neglected by assuming $n \gg 1$ and the parameter ω_n is the resonant frequency of the eigenmodes of order n in the absence of damping:

$$\omega_n = \sqrt{\frac{n\omega_{pl}^2}{n\varepsilon_\infty + (n+1)\varepsilon_2}}. \tag{4.6}$$

The system energy can be partitioned at any instant in time into potential energy $U_{n,m}(t)$ and kinetic energy $K_{n,m}(t)$, which can be expressed in terms of initial phase-space coordinates $\left[P_{n,m}(0), \dot{P}_{n,m}(0) = (\partial_t P_n)_{t=0}\right]$. As the system evolves, energy is exchanged between these two forms. Two complementary situations of particular interest are the initial conditions $\dot{P}_{n,m}(0) = 0$ and $P_{n,m}(0) = 0$:

$$\begin{cases} \dot{P}_{n,m}(0) = 0, \\ U_{n,m}(0) = \dfrac{nR^3\omega_n^2}{4\varepsilon_0\omega_{pl}^2} \left[P_{n,m}(0)\right]^2, \\ K_{n,m}(0) = 0, \end{cases} \tag{4.7}$$

$$\begin{cases} \dot{P}_{n,m}(0) = 0, \\ U_{n,m}(0) = 0, \\ K_{n,m}(0) = \dfrac{nR^3}{4\varepsilon_0 \omega_{pl}^2} \left[\dot{P}_{n,m}(0)\right]^2. \end{cases} \tag{4.8}$$

In the first state, as described by Eq. (4.7), the system energy is purely potential and it is explicitly dependent on ω_n, a function of the background permittivity ε_2. This energy corresponds to the energy of the surface polarization charge due to the (n,m) component of the polarization density (4.4) within the corresponding eigenmode electric potential $V_{n,m}^{(e,o)}(\mathbf{r},t)$:

$$V_{n,m}^{(e,o)}(r = R, \theta, \phi, t) = \frac{P_{n,m}^{(e,o)}(t) R}{\varepsilon_0 \varepsilon_2 + n\varepsilon_0 (\varepsilon_2 + \varepsilon_\infty)} Y_{n,m}^{(e,o)}(\theta, \phi). \tag{4.9}$$

We deduce from Eq. (4.9) that a decrease in the background permittivity ε_2 results in an increase in the potential energy of the system. Inversely, an increase in ε_2 reduces the potential energy of the system. If ε_2 could be instantaneously reduced to $\varepsilon_2 - d\varepsilon_2$ then the characteristic modal frequency would increase from ω_n to $\omega_n + d\omega_n$. Such an increase in the modal frequency causes the energy of the entire system to increase by:

$$dU_{n,m} \sim 2\frac{U_{n,m}}{\omega_n} d\omega_n = \left(1 + \frac{1}{n}\right) \frac{\omega_n^2 U_{n,m}}{\omega_{pl}^2} d\varepsilon_2. \tag{4.10}$$

Thus, the increase in system energy that results from the parametric modulation is proportional to the instantaneous potential energy stored within the plasmonic mode.

On the other hand, when the system is in a purely kinetic state (4.8), the total energy does not explicitly depend on the modal frequency ω_n, nor the background permittivity ε_2. An instantaneous modification of the system parameters affecting only the characteristic modal frequency would not alter the system's total energy in this state. Therefore, we identify a periodic modulation scheme of such parameters in which energy is delivered to the system by reducing ε_2 during the state of pure potential energy and increasing ε_2 during the state of pure kinetic energy. This approach

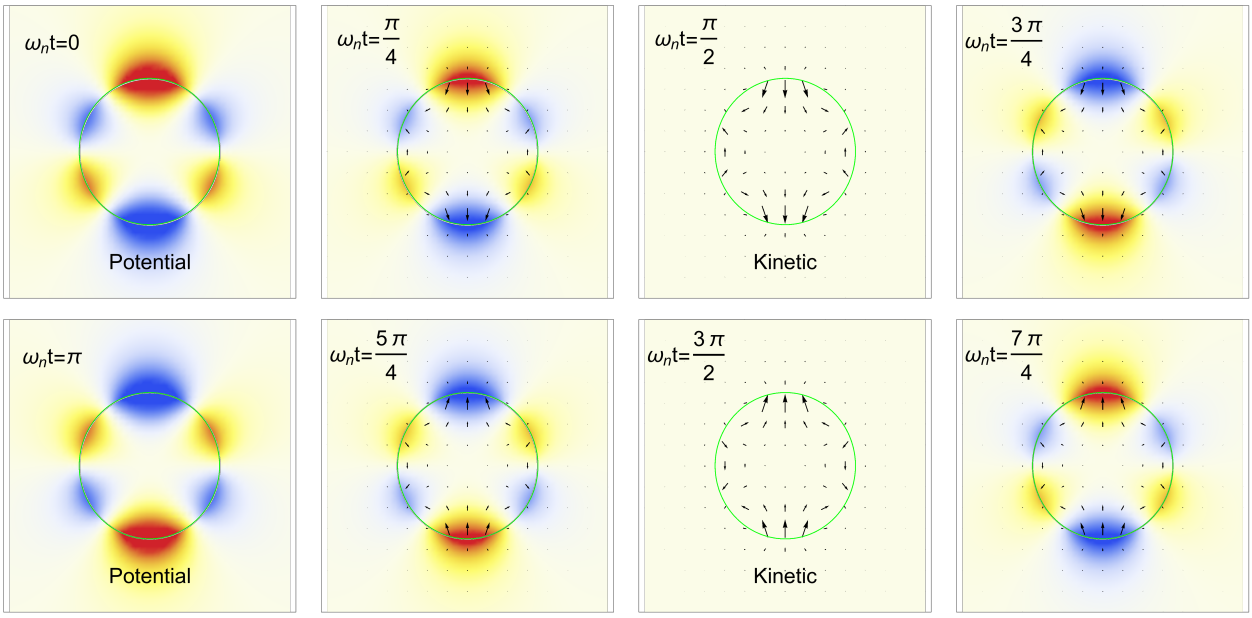

Figure 4.4: Time evolution of potential and currents of the octupolar mode of a plasmonic sphere

enables delivery of energy to the plasmonic mode without direct excitation of the charge carriers by a spatially and temporally matched external field.

By analyzing the energy dynamics of a full modulation period, we can determine a threshold in modulation depth for eigenmode order (n,m) that corresponds to parametric regeneration. Consider the initial state of a system beginning at time $t = 0$ with total energy $W_{n,m}(0)$ stored as potential energy of a plasmonic eigenmode of order (n,m). This state is identified by:

$$P_{n,m}(0) = \frac{4\varepsilon_0 \omega_{pl}^2}{nR^3 \omega_n^2} W_{n,m}(0),$$

$$\dot{P}_{n,m}(0) = 0.$$

The system oscillates freely at $\Omega_n^2 = \omega_n^2 - \gamma^2/4$, evolving to a state of pure kinetic energy $K_{n,m}(T_1) = W_{n,m}(0)e^{-\gamma T_1}$ after time $T_1 = [\pi - \arctan(2\Omega_n/\gamma)]/\Omega_n$. At this point, the phase-space coordinates are $P_{n,m}(T_1) = 0$ and $\dot{P}_{n,m}(T_1) = -P_{n,m}(0)\omega_n e^{-\gamma T_1/2}$. If the system's parameters are instantaneously modified so as to lower the eigenfrequency from ω_n to $\Theta_n = \omega_n - d\omega_n$, then no energy is transferred to or removed from the system in accordance with Eq. (4.10) since the potential energy is zero. Now oscillating at Θ_n, the system continues back to a state of pure potential energy after an

additional time $T_2 = (1/\theta_n)\arctan(2\theta_n/\gamma)$ with $\theta_n^2 = \Theta_n^2 - \gamma^2/4$. At time $T = T_1 + T_2$, the potential energy is $U_{n,m}(T) = W_{n,m}(0)e^{-\gamma T}$. If at time $T^+ = T + dt$ such that $dt \to 0$, the system's parameters are instantaneously modulated to restore the frequency of oscillation back to its initial value of ω_n, then the energy of the plasmonic mode increases to

$$W_{n,m}(T^+) = W_{n,m}(0)\left(\omega_n^2/\Theta_n^2\right)e^{-\gamma T}. \tag{4.11}$$

Finally, we equate Eq. (4.11) with the initial total energy $W_{n,m}(0)$ and solve for the threshold condition of parametric resonance regeneration. The threshold value of the modulation depth $d\omega_n$ is

$$\frac{d\omega_n}{\omega_n} = \frac{\pi}{2}\frac{\gamma}{\omega_n}. \tag{4.12}$$

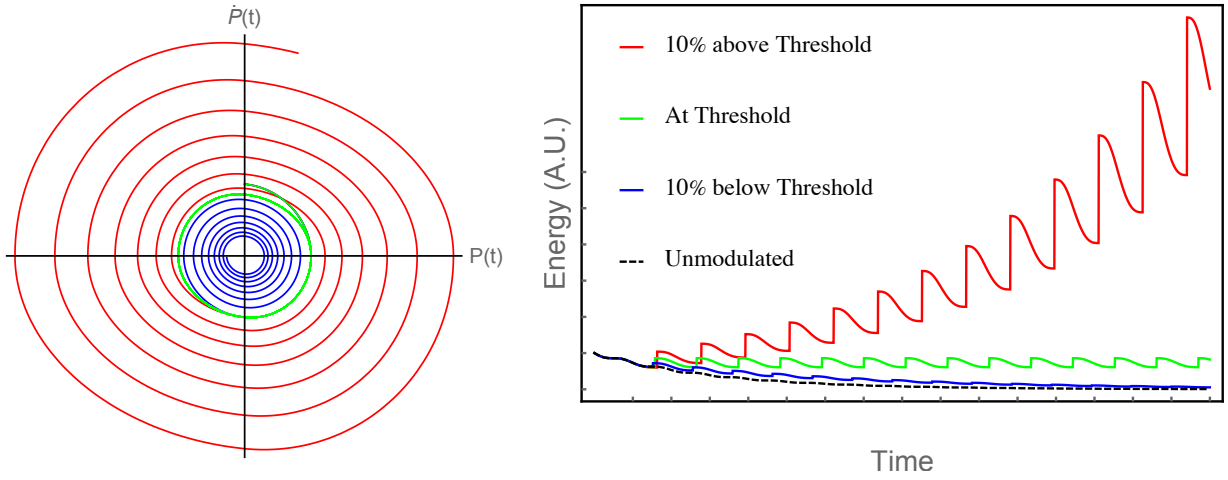

(a) Phase-space trajectory

(b) Time evolution of energy

Figure 4.5: (a) Phase-space trajectories in terms of polarization amplitude and current. (b) Temporal evolution of the total energy in a plasmonic mode under various modulation depths. When the PPR threshold represented by the green curve is exceeded, the plasmonic mode experiences a net gain in energy with increasing polarization.

The phase-space trajectory of the parametrically driven plasmonic system is illustrated in Fig. 4.6a for various modulation depths. The closed orbit, in green, represents the threshold of parametric regeneration and separates the inward and outward spiraling trajectories that respectively occur below and above the threshold. The total energies of the plasmonic mode are shown in Fig

4.6b with corresponding colors representing the various modulation depths. It is in Fig 4.6b that we identify the parametric energy transfer described by Eq. (4.10). The discontinuities that occur when the polarization amplitude (potential energy) is at a maximum and the polarization current density (kinetic energy) is zero allow the system to experience an increase in total energy through modulation of its parameters. Each additional occurrence of energy transfer is proportional to the respective instantaneous potential energy of the mode. With each iteration building upon the last, the result is a temporal energy function with an exponentially growing envelope.

The stepwise parametric modulation scheme described is an effective tool of illustration and has been useful in determining an analytical lower bound for the plasmonic regeneration threshold. However, it is impractical to assume that this idealization can be achieved in real systems, particularly at optical frequencies. A more realistic description of a physical system must include the specific temporal profile of the modulated modal frequency $\omega_n(t)$, driven by continuous transitions of parameter values over finite durations of time. This temporal variation in parameters will depend on the mechanism exploited in altering the background permittivity ε_2.

4.3 Practical Implementation

A realizable system that experiences plasmonic resonances at optical frequencies is limited to action by optical nonlinearities of electronic origin. Mechanisms that operate on longer timescales will not be sufficiently fast-acting for efficient energy transfer via PPR. A practical example of such a mechanism for modulating ε_2 is to exploit its second-order nonlinear susceptibility $\chi^{(2)}$ in the presence of a spatially uniform pump. This is an inherently anisotropic interaction due to the noncentrosymmetric material requirements of second-order optical nonlinearities. Therefore, particular care must be given in assessing the selection rules that govern what modes can interact with a given pump field.

We approach this scenario by assuming that medium 2 is endowed with second-order nonlinearity with a dominant term $\chi^{(2)}_{zzz}$. Under such hypotheses, the polarization density $\mathbf{P}_2(\mathbf{r}, t)$ in

medium 2 can be expressed in terms of the total local field $\mathbf{E}_2(\mathbf{r}, t)$ as follows:

$$\mathbf{P}_2(\mathbf{r},t) = \varepsilon_0(\varepsilon_2 - 1)\mathbf{E}_2(\mathbf{r},t) + \mathbf{P}_2^{NL}(\mathbf{r},t) \tag{4.13}$$

In Eq. (4.13), $\mathbf{P}_2^{NL}(\mathbf{r},t) = \varepsilon_0\chi^{(2)} \cdot \mathbf{E}_2(\mathbf{r},t) : \mathbf{E}_2(\mathbf{r},t)$ is the nonlinear polarization density due to the quadratic nonlinearity of medium 2. The total electric field $\mathbf{E}_2(\mathbf{r}, t)$ in medium 2 is the sum of all of the fields due to the plasmonic modes of the particle and a spatially uniform incident field $\mathbf{E}_\mathbf{P}(t)$, henceforth referred to as "pump."

We pick up where we left off at Eq. (4.4), performing similar expansions for all field quantities in terms of spherical harmonics and applying the boundary conditions at the particle's interface. This yields the following evolution equation for the polarization density amplitude associated with any of the electromagnetic angular momentum eigenmodes of the sphere:

$$\frac{d^2\mathbf{P}_{n,m}^{(e,o)}(t)}{dt^2} + \gamma\frac{d\mathbf{P}_{n,m}^{(e,o)}(t)}{dt} + \omega_n^2\mathbf{P}_{n,m}^{(e,o)}(t) = \omega_n^2\frac{S_{n,m}^{(e,o)}(t)}{n}, \tag{4.14}$$

where ω_n is the same as previously described in Eq. (4.6).

The term $S_{n,m}^{(e,o)}(t)$ on the right-hand side of Eq. (4.14) is the projection on the spherical harmonic $Y_{n,m}^{(e,o)}(\theta,\phi)$ of the nonlinear polarization density $\mathbf{P}_2^{NL}$ evaluated over the surface of the sphere:

$$S_{n,m}^{(e,o)}(t) = \oint_{\mathbf{r}=R} Y_{n,m}^{(e,o)}\mathbf{P}_2^{NL}(R,\theta,\phi,t)\cdot\hat{\mathbf{r}}\,\sin(\theta)d\theta d\phi. \tag{4.15}$$

Through (4.15), various eigenmodes are nonlinearly coupled to one another and to the pump field. The symmetry group of medium 2 and the spatial profile of the pump determine which specific three-wave mixing products contribute to the dynamics of a given eigenmode.

Let us consider the dynamics of the azimuthally uniform ($m = 0$) resonant mode of order n in the presence of a spatially uniform time-harmonic z-polarized pump $E_P(t)$. In this case, the

evolution of Eq. (4.14) assumes the following form:

$$\frac{d^2\mathbf{P}_{n,0}^{(e)}(t)}{dt^2}+\gamma\frac{d\mathbf{P}_{n,0}^{(e)}(t)}{dt}+\left[\omega_n^2-\alpha_1 E_P(t)\right]P_{n,0}^{(e)}(t)=\alpha_2\left[P_{n,0}^{(e)}(t)\right]^2. \tag{4.16}$$

The term $\alpha_1 E_p(t)P_{n,0}^{(e)}$ in Eq. (4.16) represents the three-wave mixing process responsible for the parametric interaction of the resonant mode with the pump. The term on the right-hand side of Eq. (4.16) accounts for the sum and difference frequency generation processes due to the plasmonic mode interacting with the background medium. The expressions of the nonlinear interaction coefficients α_1 and α_2 are given by

$$\alpha_1=-\frac{4\sqrt{\pi}\chi_{zzz}^{(2)}}{n\sqrt{3}}\frac{\omega_n^4}{\omega_{pl}^2}G_{n,0}^{(e,e)};\quad \alpha_2=\frac{\chi_{zzz}^{(2)}\omega_n^6}{n\varepsilon_0\omega_{pl}^4}F_{n,0}^{(e,e,e)},$$

$$F_{n,0}^{(e,e,e)}=\int_0^{2\pi}\int_0^{\pi}\left\{\cos\theta\frac{\partial}{\partial z}\left[\frac{R^{n+2}}{r^{n+1}}Y_{n,0}^{(e)}(\theta,\phi)\right]_R\times\frac{\partial}{\partial z}\left[\frac{R^{n+2}}{r^{n+1}}Y_{n,0}^{(e)}(\theta,\phi)\right]_R Y_{n,0}^{(e)}(\theta,\phi)\right\}\sin\theta d\theta d\phi,$$

$$G_{n,0}^{(e,e)}=\int_0^{2\pi}\int_0^{\pi}\left\{\cos\theta\frac{\partial}{\partial z}\left[r\,Y_{1,0}^{(e)}(\theta,\phi)\right]_R\times\frac{\partial}{\partial z}\left[\frac{R^{n+2}}{r^{n+1}}Y_{n,0}^{(e)}(\theta,\phi)\right]_R Y_{n,0}^{(e)}(\theta,\phi)\right\}\sin\theta d\theta d\phi. \tag{4.17}$$

The PPR threshold is minimized [39] if the pump field oscillates at the second-harmonic frequency of the mode of interest. This can be intuitively recognized by considering the phase states of pure potential and pure kinetic energies in Fig. 4.4. Energy is most efficiently delivered during the states of pure potential, at $\omega_n t=0$ and $\omega_n t=\pi$, while the modulation must return to the opposite extreme of oscillation during the states of pure kinetic energy; this avoids removing energy from the plasmonic mode during the rebound. The outcome is the requirement that the parametric modulation must occur twice within the period of the targeted mode for maximum energy transfer efficiency. We start, therefore, by considering a spatially uniform pump field of the form $E_P(t)=A_p\sin(2\omega_n t)$. The linear interaction of this pump with the subwavelength particle is essentially that of an electric dipole [29]. A significant observation is that the pump field at $2\omega_n$ is strongly detuned from any of the possible resonant modes, including the dipolar one at ω_1. Thus, a

relatively small absorption of the pump should be expected. In the absence of nonlinear processes, the linear absorption cross section of a subwavelength particle of volume V at the pump frequency is

$$\sigma_{2\omega_n} = \frac{36V\varepsilon_0\eta\left(\omega_n^2-\omega_1^2\right)^2\omega_{pl}^2\gamma}{(n-1)^2\left(4\omega_n^2-\omega_1^2\right)^2\omega_n^2}. \tag{4.18}$$

It is easily discerned from Eq. (4.18) that the large detuning of the pump frequency $2\omega_n$ from the dipolar resonance of the plasmonic mode at ω_1 results in a negligibly small absorption cross section. This confirms the expectation of minimal pump absorption within the linear regime. Therefore, we consider the nonlinear response to describe how absorption increases dramatically when the PPR threshold is met and exceeded. In solving Eq. (4.16), we notice that so long as the condition $\left|P_{n,m}^{(e,o)}(t)\right| \ll \alpha_1 A_p/\alpha_2$ holds, which is the case at the initial stages of the parametric interaction, a solution can be easily obtained in terms of Mathieu functions [3, 31]. More intuitive though is the following slowly varying envelope approximate solution:

$$P_{n,m}^{(e,o)}(t) = p(t)\cos\left[\omega_n t-\theta(t)\right]e^{-\frac{\gamma t}{2}},$$

$$p(t) = p_0\sqrt{\cosh\left(\frac{\alpha_1 A_p}{2\omega_n}t\right)}; \quad \theta(t) = \operatorname{arccot}\left[\exp\left(-\frac{\alpha_1 A_p}{2\omega_n}t\right)\right] \tag{4.19}$$

where p_0 is the initial modal amplitude. From Eq. (4.19), for $p(t)$, it is clear that the system enters the PPR regime provided that the pump electric-field amplitude A_p exceeds the threshold value: $A_{PPR} = 2\gamma\omega_n/\alpha_1$.

It is worth pointing out a unique property of plasmonic parametric gain that emerges from the analysis above: a plasmonic mode of any order *(m,n)* can undergo PPR and be amplified by a *spatially uniform* modulation of the background permittivity, provided that the corresponding threshold is exceeded. This is in contrast with conventional LSP resonances, which, for a mode of order *(m,n)*, require a driving field with a matching spatial profile — a condition almost impossible to realize in practice for high-order plasmonic modes of deeply sub-wavelength particles. For these reasons PPR is uniquely suitable to access plasmonic resonances of arbitrarily high order in deeply

sub-wavelength structures.

4.4 Plasmonic Parametric Absorbers

The unique characteristics of PPR lend themselves to interesting applications in optical limiting. Recently, of a new class of nonlinear absorbers termed Plasmonic Parametric Absorbers (PPA) has been proposed [20]. The key insight informing the PPA idea is that in the PPR process the pump field experiences an absorption rate that strongly depends on the intensity of the pump itself, creating two distinct regimes: one of weak absorption under low intensity illumination and one of strong absorption when the threshold of parametric resonance is reached or exceeded. Such a threshold condition separates distinct dynamics, so that $P_{n,m}^{(e,o)}(t)$ decreases exponentially for $A_p < A_{PPR}$ and increases exponentially for $A_p > A_{PPR}$. Such contrasting modal dynamics are reflected in the distinct absorption regimes to which the pump is subjected. As shown in Ref. [20], the power parametrically transferred from the pump to the resonant mode is given by

$$W_{abs}(t) = \frac{nR^3\alpha_1 A_p p_0^2}{32\varepsilon_0\omega_{pl}^2}\left[2\omega_n + \gamma\sinh\left(\frac{\alpha_1 A_p t}{2\omega_n}\right)\right]e^{-\gamma t} \sim \frac{nR^3\alpha_1 A_p p_0^2\gamma}{64\varepsilon_0\omega_{pl}^2}\exp\left[(A_p - A_{PPR})\frac{\alpha_1 t}{2\omega_n}\right]. \tag{4.20}$$

Equation (4.20) highlights the fundamental trait of PPA: in PPA, absorption is vanishingly small for incident fields below the PPR threshold and increases exponentially under high-intensity conditions. This is in stark contrast with linear absorption.

Saturation of the exponential behavior is clearly expected because, if nothing else, the absorbed power of Eq. (4.20) cannot exceed the finite power carried by the pump. In reality, a different mechanism limits the power absorbed. This mechanism is the resonance detuning caused by additional three-wave mixing processes in Eq. (4.16) that have been neglected thus far. As $\left|P_{n,m}^{(e,o)}(t)\right| \sim \alpha_1 A_p/\alpha_2$, Eq. (4.16) can only be integrated numerically. Nevertheless, the following asymptotic expressions for $P_{n,m}^{(e,o)}(t)$ as $t \to \infty$ hold for $A_p > A_{PPR}$:

$$P_{n,m}^{(e,o)}(t) \sim -\frac{\alpha_2 Q_1^2}{2\omega_n^2} + Q_1\cos(\omega_n t + \theta_1) + \frac{\alpha_2 Q_1^2}{6\omega_n^2}\cos(2\omega_n t + 2\theta_1)$$

$$\theta_1 = \frac{1}{2}\arccos\left(-\frac{A_{PPR}}{A_p}\right); \quad Q_1 = \frac{\omega_n}{\alpha_2}\sqrt{\frac{6\gamma\omega_n}{5}\sqrt{\left(\frac{A_p}{A_{PPR}}\right)^2 - 1}}. \tag{4.21}$$

Within the range of validity of Eq. (4.21), the exponentially growing oscillations of the polarization density amplitude level off as $t \to \infty$ after a sequence of relaxation oscillations. In Fig. 4.6, the numerical solution of Eq. (4.16) (indicated in blue) is compared with the predictions of the asymptotic model in Eq. (4.21), shown in orange.

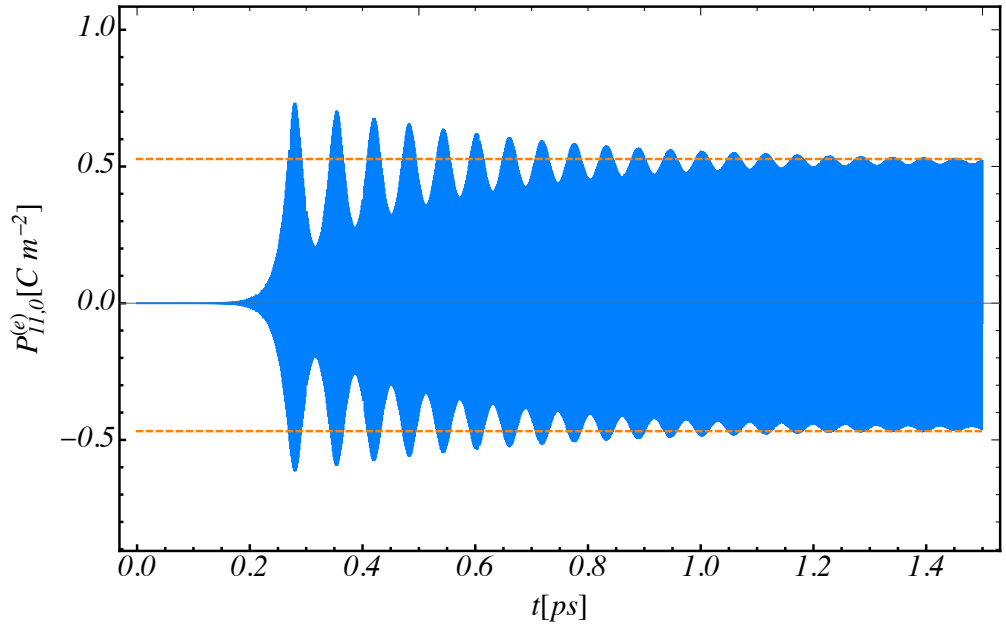

Figure 4.6: Polarization density amplitude term $P^{(e)}_{11,0}$ of a silver sphere immersed in an MNA background medium. In order to better highlight the relaxation oscillations occurring in the system, we show a case in which the PPR threshold is exceeded by a large margin ($A_p = 20A_{PPR}$). The dashed lines show the oscillation limits predicted by the asymptotic Eq. (4.20).

Based on Eq. (4.21), the average power $\overline{W}_P$ transferred from the pump to the plasmonic mode asymptotically approaches the value

$$\overline{W}_{abs}(t \to \infty) = \frac{3}{20}nR^3\frac{\gamma}{\varepsilon_0\omega_{pl}^2}\frac{\omega_n^3}{\alpha_2^2}\sqrt{\left(\frac{A_p}{A_{PPR}}\right)^2 - 1}. \tag{4.22}$$

Using the steady-state asymptotic estimate of the absorbed power, Eq. (4.22), it is possible to obtain the PPR contribution to the particle absorption cross-section [in addition to the linear term

from Eq. (4.18)]:

$$\sigma_{NL} = \frac{3nR^3\omega_n^3}{40\varepsilon_0\sqrt{\varepsilon_2}\omega_{pl}^2}\frac{\alpha_1^2}{\alpha_2^2}\sqrt{\frac{I_{PPR}}{I_p}\left(1-\frac{I_{PPR}}{I_p}\right)}, \quad I_p > I_{PPR}. \tag{4.23}$$

In Eq. (4.23), $I_p = A_p^2/(2\eta)$ is the incident intensity and $I_{PPR} = A_{PPR}^2/(2\eta)$ is the PPR intensity threshold, where η is the intrinsic impedance of the background medium. If particles similar to the one described thus far are dispersed with density N in the background medium, the nonlinear pump attenuation coefficient of the composite follows from Eq. (4.23) as $\alpha_{NL} = N\sigma_{NL}$.

Figure 4.7 shows how the normalized absorption cross-section of a silver sphere of radius $R =$ 100nm in an MNA [34, 16] host is affected by various modes undergoing PPR. The absorption cross-section is plotted against the normalized pump intensity and, for each of the PPR modes considered in Fig. 4.7, the incident pump field is at twice the value of the corresponding resonant frequency given by Eq. (4.6). For the case at hand, all the possible PPR resonant wavelengths λ_n fall in the range $\lambda_\infty < \lambda_n \leq \lambda_1$, where $\lambda_\infty = 563$nm and $\lambda_1 = 448$nm.

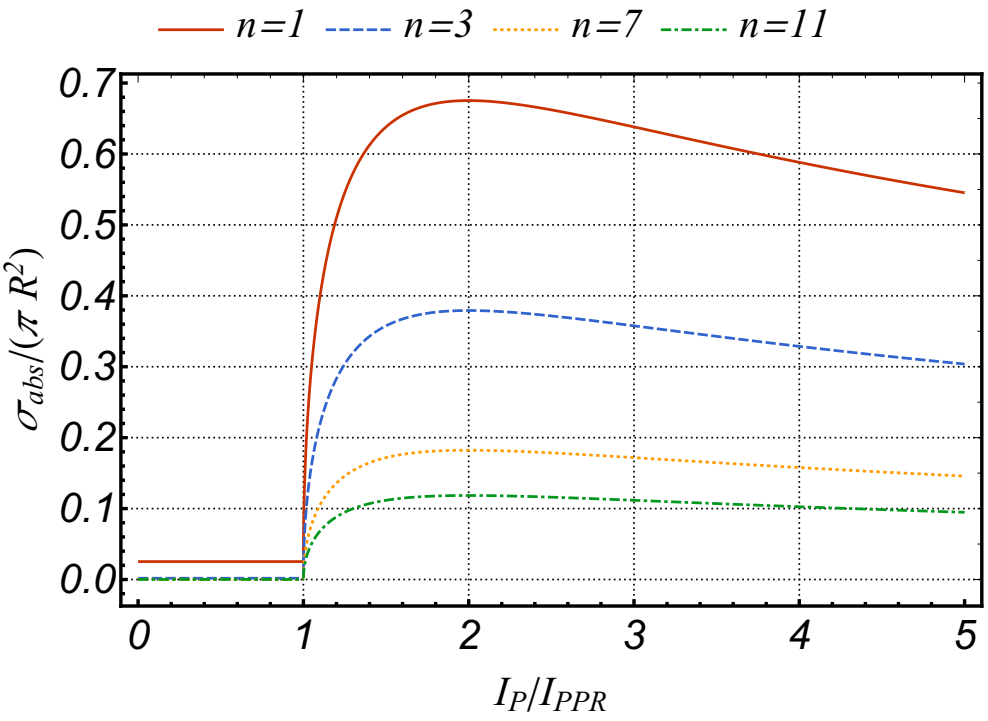

Figure 4.7: Absorption cross-section of the plasmonic particle normalized to the geometrical cross-section as a function of the incident intensity.

As is evident from Fig. 4.7, as soon as a pump field of frequency $2\omega_n$ exceeds the intensity threshold I_{PPR}, the particle's absorption cross-section increases dramatically due to the contribution of the mode of eigenfrequency ω_n undergoing PPR. It is difficult to discern via the linear plot but the higher order modes increase in cross-section by several orders of magnitude. This phenomenon is a form of reverse saturable absorption and may, therefore, be of interest in optical limiting devices, especially given the design versatility of metallic nanoparticles for targeting different spectral regions.

For the purpose of illustration, in Fig. 4.8, we apply the analysis and the models described thus far to the practically relevant case of a pulsed pump. The pulse considered here is a 30ps pulse of average power 0.5W, focused to an area of 25 μm^2, on parametric resonance with the $n = 11,\ m = 0$ mode ($\lambda_{11} = 460$nm) of a silver particle of radius 100nm embedded in an MNA background medium. The orange curve in Fig 4.8 shows the total instantaneous power of the pump field. The blue curve shows the instantaneous absorbed power caused by the PPR process. The vertical dashed lines show the time interval in which the pump field exceeds the PPR threshold.

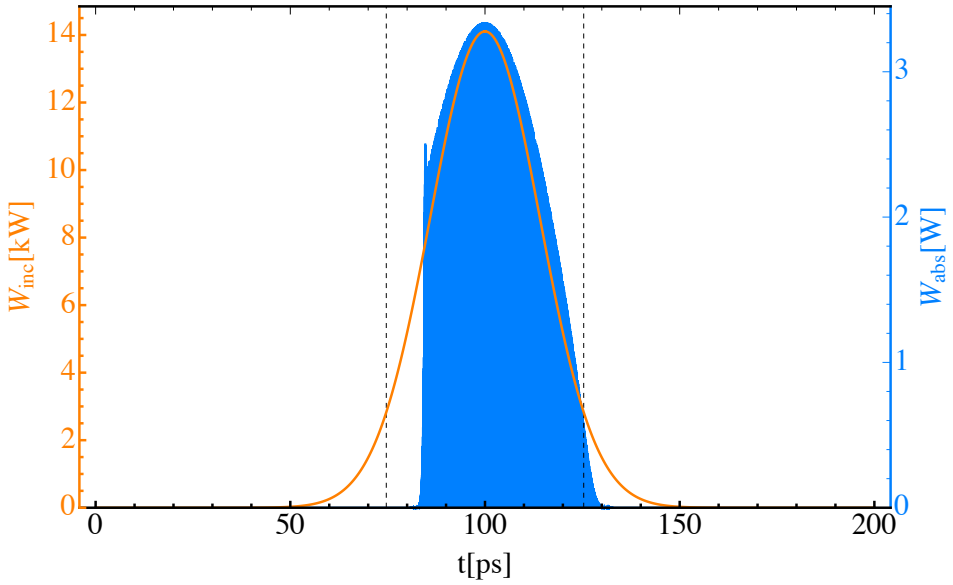

Figure 4.8: Orange curve shows instantaneous pump power W_{inc}. The blue curve shows the instantaneous pump power W_{abs} absorbed by the particle via PPR of the $n = 11, m = 0$ mode. The dashed vertical lines indicate the times at which the pump intensity is equal to the PPR threshold.

A similar behavior is observed both in Figs. 4.6 and 4.8 at the onset of PPR, where the modal polarization (and the corresponding absorption) builds up exponentially to slightly surpass the steady-state value and then relaxes to such a value through a series of oscillations (only one is discernible in Fig 4.8). Fig 4.8 confirms the dramatic increase in absorption that PPAs exhibit under high-intensity illumination. In a similar example from Ref. [20], the PPR threshold occurs at an incident fluence of $F_{PPR} \sim 0.2\text{J/cm}^2$. The background medium, MNA, has been shown to withstand these levels of radiation by Mayy et al. [32] and smooth silver surfaces have been shown to endure such fluence levels as well [48]. This suggests that the proposed materials are suitable for building PPR-based optical limiting devices within the ascribed parameters without fear of catastrophic failure or irreversible damage.

4.5 Caveats and Future Research

It should be brought to attention that the proposed arrangement of a single 100nm silver sphere embedded in MNA provides an excellent basis for the analysis of PPA, but does not, by itself, make for an ideal optical limiter. The most obvious of limitations is the narrow bandwidth of modes available for PPR. This is easily overcome by the inclusion of a variety of shapes and sizes of plasmonic particles that will expand the resonant frequency range of plasmonic modes available within the active medium. We point out that, so long as these particles remain deeply subwavelength, the governing mechanisms of the PPR action remain the same. Additional enhancements to the bandwidth of the limiting response may be made through an arrangement of layered media whose thicknesses vary on the order of the wavelength (e.g. phase matching).

The second limitation that we consider is the polarization sensitivity of the nonlinear susceptibility term $\chi^{(2)}$ that mediates the background permittivity. This is an obvious constraint on the orientation of threats that can be effectively absorbed by the limiter. Again, a possible solution is to layer multiple slabs of media—this time having been rotated incrementally such that their axes of greatest $\chi^{(2)}$ response vary sufficiently. Another solution may be to investigate centrosymmetric crystalline materials whose $\chi^{(3)}$ susceptibility is on the order of the second-order MNA response

at 500pm/V [16, 32]. Significant reduction of this nonlinear refraction in the background medium will decrease the modulation depth of the eigenfrequency, thereby increasing the PPR threshold and the limiting level of the device. Of similar concern is the frequency dependence of this change in refractive index. Whatever background material is chosen must maintain a sufficiently deep modulation of its permittivity across the bandwidth of intended effective limiting.

We have not evaluated the nature of thermal dissipation in these media and suggest further investigation along these lines in order to quantify their maximum limiting abilities before failure. Photolysis of the nanoparticles is another possible concern that remains yet to be analyzed as it is a complex issue that requires one to account for detailed morphology of the particles [20]. Finally, we note that the specific heterogeneous medium described in this document is only capable of limiting wavelengths beyond the visible spectrum, in the ultraviolet. While this certainly has numerous potential applications, limiting in the visible range is highly desirable as well. A PPA device with such capability requires design considerations outside of typical limiting materials due to the fact that the plasmonic modes must oscillate at eigenfrequencies $\sim 1/2$ of those being targeted for limiting. It is for this reason that we suggest further investigation into pairings of plasmonic particles and dielectric media whose plasmonic modes exist in the near-infrared.

In conclusion, we have illustrated the principles of the operation of PPR and how they pertain to optical limiting. Unlike conventional LSP resonances, all of the plasmonic modes of a nanostructure, including the strongly sub-radiant ones, can be resonantly excited by spatially uniform optical pumping, provided that the corresponding threshold is exceeded. Accessing such a high density of strongly localized states holds promise for enhancing nonlinear light–matter interaction at the nanoscale for the development of nonlinear optical metamaterials as well as for optical limiting applications. In the context of PPR, we have discussed the closely related theory of PPAs. PPAs exhibit a reverse saturable absorption behavior whereby an incident field that is parametrically resonant with one or more of the modes of a plasmonic particle experiences a strongly enhanced absorption whenever its intensity exceeds the relevant PPR threshold. Such an effect makes PPAs very promising candidates for optical limiting applications, in addition to being of fundamental

interest in the emerging field of nonlinear plasmonics.

References

[1] Allan, G. R., Labergerie, D. R., Rychnovsky, S. J., Boggess, T. F., Smirl, A. L., & Tutt, L. (1992). Picosecond reverse saturable absorption in King's complex [(C5h5)Fe(CO)]4. *The Journal of Physical Chemistry*, 96(15), 6313–6317.

[2] Arbogast, J. W., Darmanyan, A. P., Foote, C. S., Diederich, F. N., Whetten, R. L., Rubin, Y., Alvarez, M. M., & Anz, S. J. (1991). Photophysical properties of sixty atom carbon molecule (C60). *The Journal of Physical Chemistry*, 95(1), 11–12.

[3] Arfken, G. B., Weber, H. J., & Harris, F. E. (2012). *Mathematical Methods for Physicists: A Comprehensive Guide*. Amsterdam ; Boston: Academic Press, 7th edition.

[4] Asher, S. A., Kesavamoorthy, R., Jagannthan, S., & Rundquist, P. (1992). New nonlinear Bragg diffraction devices. In *Nonlinear Optics III*, volume 1626 (pp. 238–242).: International Society for Optics and Photonics.

[5] Auston, D. H., McAfee, S., Shank, C. V., Ippen, E. P., & Teschke, O. (1978). Picosecond spectroscopy of semiconductors. *Solid-State Electronics*, 21(1), 147–150.

[6] Bergman, D. J. & Stockman, M. I. (2003). Surface Plasmon Amplification by Stimulated Emission of Radiation: Quantum Generation of Coherent Surface Plasmons in Nanosystems. *Physical Review Letters*, 90(2), 027402.

[7] Blau, W., Byrne, H., Dennis, W. M., & Kelly, J. M. (1985). Reverse saturable absorption in tetraphenylporphyrins. *Optics Communications*, 56(1), 25–29.

[8] Boggess, T., Bohnert, K., Mansour, K., Moss, S., Boyd, I., & Smirl, A. (1986). Simultaneous measurement of the two-photon coefficient and free-carrier cross section above the bandgap of crystalline silicon. *IEEE Journal of Quantum Electronics*, 22(2), 360–368.

[9] Boggess, T., Smirl, A., Moss, S., Boyd, I., & Van Stryland, E. (1985). Optical limiting in GaAs. *IEEE Journal of Quantum Electronics*, 21(5), 488–494.

[10] Boggess, T. F., Allan, G. R., Rychnovsky, S. J., Labergerie, D. R., Venzke, C. H., Smirl, A. L., Tutt, L. W., Kost, A. R., McCahon, S. W., & Klein, M. B. (1993). Picosecond investigations of optical limiting mechanisms in King's complex. *Optical Engineering*, 32(5), 1063–1068.

[11] Boggess, T. F., Bohnert, K., Norwood, D. P., Mire, C. D., & Smirl, A. L. (1987). Nonlinear refraction in silicon induced by one-micron picosecond pulses. *Optics Communications*, 64(4), 387–392.

[12] Boggess, T. F., Moss, S. C., Boyd, I. W., & Smirl, A. L. (1984). Nonlinear-optical energy regulation by nonlinear refraction and absorption in silicon. *Optics Letters*, 9(7), 291–293.

[13] Brandelik, D., McLean, D., Schmitt, M., Epling, B., Colclasure, C., Tondiglia, V., Pachter, R., Obermeier, K., & Crane, R. L. (1992). Nonlinear Optical Properties of Buckminsterfullerene Solutions. *MRS Online Proceedings Library Archive*, 247.

[14] Butikov, E. I. (2015). *Simulations of Oscillatory Systems: with Award-Winning Software, Physics of Oscillations*. Boca Raton: CRC Press, 1st edition.

[15] Cang, H., Salandrino, A., Wang, Y., & Zhang, X. (2015). Adiabatic far-field sub-diffraction imaging. *Nature Communications*, 6(1), 1–6.

[16] Chlema, D. (1987). *Nonlinear Optical Properties of Organic Molecules and Crystals*, volume 1. Academic Press, 1st edition.

[17] Coulter, D. R., Miskowski, V. M., Perry, J. W., Wei, T.-H., Stryland, E. W. V., & Hagan, D. J. (1989). Optical Limiting In Solutions Of Metallo-Phthalocyanines And Naphthalocyanines. In *Materials for Optical Switches, Isolators, and Limiters*, volume 1105 (pp. 42–51).: International Society for Optics and Photonics.

[18] Cronin-Golomb, M. & Yariv, A. (1985). Optical limiters using photorefractive nonlinearities. *Journal of Applied Physics*, 57(11), 4906–4910.

[19] Eaton, D. F. (1991). Nonlinear Optical Materials. *Science*, 253(5017), 281–287.

[20] Fardad, S. & Salandrino, A. (2018). Plasmonic parametric absorbers. *Optics Letters*, 43(24), 6013–6016.

[21] Geusic, J. E., Singh, S., Tipping, D. W., & Rich, T. C. (1967). Three-Photon Stepwise Optical Limiting in Silicon. *Physical Review Letters*, 19(19), 1126–1128.

[22] Giuliano, C. & Hess, L. (1967). Nonlinear absorption of light: Optical saturation of electronic transitions in organic molecules with high intensity laser radiation. *IEEE Journal of Quantum Electronics*, 3(8), 358–367.

[23] Hagan, D. J., Stryland, E. W. V., Wu, Y. Y., Wei, T. H., Sheik-Bahae, M., Said, A., Mansour, K., Young, J., & Soileau, M. J. (1989). Passive Broadband High Dynamic Range Semiconductor Limiters. In *Materials for Optical Switches, Isolators, and Limiters*, volume 1105 (pp. 103–113).: International Society for Optics and Photonics.

[24] Kauranen, M. & Zayats, A. V. (2012). Nonlinear plasmonics. *Nature Photonics*, 6(11), 737–748.

[25] Khoo, I.-C., Lindquist, R. G., Jr, R. R. M., Mansfield, R. J., Zhou, P., & LoPresti, P. G. (1990). Picosecond-millisecond optical nonlinearities of liquid crystals for limiting and switching applications. In *Electro-Optical Materials for Switches, Coatings, Sensor Optics, and Detectors*, volume 1307 (pp. 336–349).: International Society for Optics and Photonics.

[26] Khoo, I. C. & Shen, Y. R. (1985). Liquid Crystals: Nonlinear Optical Properties And Processes. *Optical Engineering*, 24(4), 244579.

[27] Kost, A., Tutt, L., Klein, M. B., Dougherty, T. K., & Elias, W. E. (1993). Optical limiting with C_{60} in polymethyl methacrylate. *Optics Letters*, 18(5), 334–336.

[28] Lund, D. J., Edsall, P. R., & Masso, J. D. (1990). Another look at saturable absorbers for laser eye protection. In *Laser Safety, Eyesafe Laser Systems, and Laser Eye Protection*, volume 1207 (pp. 193–201).: International Society for Optics and Photonics.

[29] Maier, S. A. (2007). *Plasmonics: Fundamentals and Applications*. New York: Springer, 2007 edition.

[30] Mansour, K., Stryland, E. W. V., & Soileau, M. J. (1990). Characterization of optical nonlinearities in carbon black suspension in liquids. In *Conference on Lasers and Electro-Optics (1990), paper CTHI40* (pp. CTHI40).: Optical Society of America.

[31] Mathieu, E. (1868). Mémoire sur le mouvement vibratoire d'une membrane de forme elliptique. *Journal de Mathématiques Pures et Appliquées*, 13, 137–203.

[32] Mayy, M., Zhu, G., Webb, A. D., Ferguson, H., Norris, T., Podolskiy, V. A., & Noginov, M. A. (2014). Toward parametric amplification in plasmonic systems: Second harmonic generation enhanced by surface plasmon polaritons. *Optics Express*, 22(7), 7773–7782.

[33] Michael, R. R., Lawson, C. M., Euliss, G. W., & Mohebi, M. (1992). Nanosecond switching in carbon microparticle suspensions. In *Nonlinear Optics III*, volume 1626 (pp. 205–216).: International Society for Optics and Photonics.

[34] Morita, R., Ogasawara, N., Umegaki, S., & Ito, R. (1987). Refractive Indices of 2-Methyl-4-Nitroaniline (MNA). *Japanese Journal of Applied Physics*, 26(10A), L1711.

[35] Nashold, K. M., Brown, R. A., Walter, D. P., & Honey, R. C. (1989). Temporal And Spatial Characterization Of Optical Breakdown In A Suspension Of Small Absorbing Particles. In *Materials for Optical Switches, Isolators, and Limiters*, volume 1105 (pp. 78–90).: International Society for Optics and Photonics.

[36] Perry, J. W., Khundkar, L. R., Coulter, D. R., Alvarez, D., Marder, S. R., Wei, T. H., Sence, M. J., Van Stryland, E. W., & Hagan, D. J. (1991). Excited State Absorption and Optical Limit-

ing in Solutions of Metallophthalocyanines. In J. Messier, F. Kajzar, & P. Prasad (Eds.), *Organic Molecules for Nonlinear Optics and Photonics*, NATO ASI Series (pp. 369–382). Dordrecht: Springer Netherlands.

[37] Rychnovsky, S. J., Allan, G. R., Venzke, C. H., Smirl, A. L., & Boggess, T. F. (1992). Optical nonlinearities and optical limiting in GaP at 532 nm. In *Nonlinear and Electro-Optic Materials for Optical Switching*, volume 1692 (pp. 191–196).: International Society for Optics and Photonics.

[38] Said, A. A., Sheik-Bahae, M., Hagan, D. J., Canto-Said, E. J., Wu, Y.-Y., Young, J., Wei, T.-H., & Stryland, E. W. V. (1990). Nonlinearities in semiconductors for optical limiting. In *Electro-Optical Materials for Switches, Coatings, Sensor Optics, and Detectors*, volume 1307 (pp. 294–301).: International Society for Optics and Photonics.

[39] Salandrino, A. (2018). Plasmonic parametric resonance. *Physical Review B*, 97(8), 081401.

[40] Sension, R. J., Phillips, C. M., Szarka, A. Z., Romanow, W. J., McGhie, A. R., McCauley, J. P., Smith, A. B., & Hochstrasser, R. M. (1991). Transient absorption studies of carbon (C60) in solution. *The Journal of Physical Chemistry*, 95(16), 6075–6078.

[41] Sheik-Bahae, M., Hagan, D. J., & Van Stryland, E. W. (1990). Dispersion and band-gap scaling of the electronic Kerr effect in solids associated with two-photon absorption. *Physical Review Letters*, 65(1), 96–99.

[42] Soileau, M. J., Stryland, E. W. V., Guha, S., Sharp, E. J., Wood, G. L., & Pohlmann, J. L. W. (1987). Nonlinear optical Properties of Liquid Crystals In The Isotropic Phase. *Molecular Crystals and Liquid Crystals*, 143(1), 139–143.

[43] Stryland, E. W. V., Vanherzeele, H., Woodall, M. A., Soileau, M. J., Smirl, A. L., Guha, S., & Boggess, T. F. (1985). Two Photon Absorption, Nonlinear Refraction, And Optical Limiting In Semiconductors. *Optical Engineering*, 24(4), 244613.

[44] Tutt, L. W. & Boggess, T. F. (1993). A review of optical limiting mechanisms and devices using organics, fullerenes, semiconductors and other materials. *Progress in Quantum Electronics*, 17(4), 299–338.

[45] Wang, N. Q., Cai, Y. M., Heflin, J. R., & Garito, A. F. (1990). Measurement of The Third Order Optical Susceptibility of Quasi-Two Dimensional Conjugated Discs: Silicon Naphthalocyanine. *Molecular Crystals and Liquid Crystals Incorporating Nonlinear Optics*, 189(1), 39–48.

[46] Wherrett, B. S. (1984). Scaling rules for multiphoton interband absorption in semiconductors. *JOSA B*, 1(1), 67–72.

[47] Wolfe, C. M., Stillman, G. E., & Holonyak, N. (1989). *Physical Properties of Semiconductors*. Englewood Cliffs, N.J. : Prentice Hall.

[48] Wood, R. M. (2003). *Laser-Induced Damage of Optical Materials*. Bristol: CRC Press, 1st edition.

[49] Zhang, S., Genov, D. A., Wang, Y., Liu, M., & Zhang, X. (2008). Plasmon-Induced Transparency in Metamaterials. *Physical Review Letters*, 101(4), 047401.